Titre: Title:	Optical power test station using and integrating sphere
Auteur: Author:	Alain Mangano
Date:	1993
Type:	Mémoire ou thèse / Dissertation or Thesis
Référence: Citation:	Mangano, A. (1993). Optical power test station using and integrating sphere [Mémoire de maîtrise, Polytechnique Montréal]. PolyPublie. https://publications.polymtl.ca/57032/

UNIVERSITE DE MONTREAL

OPTICAL POWER TEST STATION USING AN INTEGRATING SPHERE

par

Alain MANGANO

DEPARTEMENT DE GENIE MECANIQUE

ECOLE POLYTECHNIQUE

RAPPORT DE PROJET PRESENTE EN VUE DE L'OBTENTION

DU GRADE DE MAITRE EN INGENIERIE (M.Ing.)

(GENIE MECANIQUE)

avril 1993

DEDICATION

To Blackie Lawless of WASP

"The Last Command - Who Dares Wins"

SUMMARY

The integrating sphere is revolutionizing the way optical power, emitted from semiconductor light sources, is measured. This optical component, replacing the traditional attenuating filter, has been adapted into an optical power test bench customized by EG&G Optoelectronics. Primarily used to evaluate high power semiconductor lasers, the integrating sphere shows its strength and versatility where the conventional set-ups are limited.

The advantage of an optical power test bench using an integrating sphere relies on the fact that a known fraction of light is sampled rather than measuring the full optical power attenuated by a filter sensitive to the incidence of light emission.

This optical power test bench is the norm against which all other optical power test benches are evaluated at EG&G Optoelectronics, in Vaudreuil, Qc. Equipped with "state of the art" current pulsers, an accurate temperature controller and well thought-out fixtures, this optical power test bench can test all devices manufactured at EG&G regardless of package geometry, test temperature, current requirements or emission wavelength.

The integrating sphere along with its exit port

extension tubes and photodetector assemblies requires a system calibration instead of the traditional component calibrations superimposed onto one another. An operational procedure was written to verify the alignment between the device under test and the inlet port of the sphere as well as verifying basic electrical interconnections and proper electrical device bias settings.

This optical power test bench was successfully designed and introduced into the manufacturing facility, where it became obvious that its accuracy of measurement and versatility could be surpassed by no other test bench. Manufacturing throughputs (parts tested/hour) on this optical power test bench are however significantly lower than that of conventional set-ups. This area still requires work.

An experiment conducted reveals that the integrating sphere is sensitive to the reflectivity of its own input and output ports which resulted in amplified throughput until these ports were shrouded with a non-reflective material. Another experiment reveals that the sphere inlet port cannot be taken as the defining aperture. This is due to the thickness of the sphere inner skin that clips the entering

light. This problem is corrected with custom fixtures. Finally a last experiment is conducted to determine the range of optical power over which both photodetector assemblies can operate linearly. These parameters are important since the operational procedure for the integrating sphere set-up must recommend the proper configuration to ensure valid measurements. What is then found is a station capable of a large variety of tests, whose limitations are defined and documented in operational and calibration procedures.

ABSTRACT

Basic operating principles of semiconductor laser diodes and photodetectors are reviewed and illustrated. The integrating sphere is introduced as a valid and preferred optical element in the characterization of optical power emitted from semiconductor light sources. The theoretical operating principles of the integrating sphere are presented as well as the factors that typically flaw the conventional optical power test benches. Great emphasis is placed on the incorporation of the integrating sphere into an optical power test bench designed from the ground up. The major topics of discussion include its mechanical layout, electrical drivers, thermal considerations, optical accessories and device fixtures. The station is reviewed as a whole and a detailed specification is presented. A specific system calibration procedure is written showing the difference with the traditional component calibrations superimposed onto one another. An operational procedure is presented to aid supervisors in setting up the station for one or more tests as well as providing assistance to operators not familiar with the equipment. Results of several experiments (throughput measurements, cone angle difficulties, and photodetector linearity) are tabulated, further characterizing the behavior of the integrating sphere test station. Corrective actions are implemented when the behavior of the sphere is shown to be unacceptable

(i.e. systematic errors in measurements). Costing for the basic station along with its many accessories, is presented to EG&G management to aid in the marketing of this new product. Actual manufacturing throughputs, for a variety of devices, are presented. A special section is set aside, outlining the faults found along with the corrective action EG&G Optoelectronics, has taken.

RESUME

La sphère d'intégration a complètement chambardé la méthode par laquelle la puissance optique, émise de sources lumineuses semiconductrices, est mesurée. Cet élément optique, avec ses accessoires, qui remplace le filtre atténuant conventionnel, s'adapte sur un banc d'essai conçu sur mesure par EG&G Optoélectronique, Vaudreuil, Qc. Utilisé à prime abord pour évaluer des sources lumineuses de haute puissance, le banc d'essais utilisant la sphère d'intégration démontre sa polyvalence et sa précision de mesure là où les bancs d'essais conventionnels commencent à démontrer leurs faiblesses.

L'avantage principal est relié au principe de l'échantillonnage précis du flux lumineux propre aux sphères d'intégration versus l'atténuation incertaine, dûe à la sensibilité des filtres aux phénomènes optiques tel que l'angle d'incidence. Le banc d'essai de puissance optique utilisant la sphère d'intégration est devenu depuis, la norme selon laquelle tout autre banc d'essai est évalué.

Equipé de sources de courant de haute technologie, d'un échangeur de chaleur et de fixtures dessinées sur mesure, ce banc d'essai peut évaluer toutes les sources lumineuses fabriquées à EG&G Optoélectronique, Vaudreuil, Qc., peu importe la géométrie du boîtier, la température ou le

courant requis ou la longueur d'onde.

La sphère d'intégration, avec ses tubes d'extension et ses photodétecteurs, requiert un étalonnage propre à chaque configuration géométrique qu'elle peut adopter. Le banc d'essai conventionnel peut se satisfaire d'un étalonnage pour chacune de ses composantes optiques. Une procédure d'utilisation à été écrite afin que le superviseur puisse vérifier l'alignement optique entre la source lumineuse et la bouche d'entrée de la sphère. Les interconnections électriques et la vérification du courant requis sont également indiquées.

Ce nouveau banc d'essai optique a été introduit sur la ligne d'assemblage où il est vite devenu évident que la précision des mesures prises et sa polyvalence ne pouvaient être surpassées par nul autre banc d'essai. Les rendements manufacturiers (pièces/heure) sont cependant inférieurs à ceux des bancs conventionnels. Il faudra travailler à l'amélioration de ce point.

Une première expérience a démontré que la bouche d'entrée de la sphère ne pouvait être considérée comme l'orifice définissant le cône de lumière qui y pénètre.

Ceci parce que la couche réflective intérieure était d'une épaisseur telle qu'elle gênait l'entrée de la lumière. Une autre expérience a démontré qu'une portion du flux lumineux incident sur le photodétecteur, fixé à la sortie de la sphère, était d'abord réfléchie sur la gorge de cette même sortie. Finalement, une dernière expérience avait pour but de déterminer sur quelle étendue les photodétecteurs opéraient de façon linéaire. Ces trois expériences étaient importantes car elles allaient définir la façon dont ce banc d'essai serait utilisé.

Des essais ont étés faits pour vérifier nos valeurs expérimentales d'échantillonnages avec ceux théoriquement proposées par le manufacturier. La difference n'est que de 3.4% entre la theorie et ce qui a été mesuré au laboratoire d'essais. Le comportement de la sphère d'intégration est donc bien défini par les procédures écrites à cette fin.

ACKNOWLEDGMENTS

A warm thank-you to:

my parents, my friends and the better part of the western world for putting up with the ramblings of a tired student

technical and support staff at EG&G

TABLE OF CONTENTS

LIST OF FIGURES

PAGE

LIST OF TABLES

PAGE

LIST OF ACRONYMS AND SYMBOLS

A	Ampere
AR	anti-reflect
CD	Compact Disc
CW	Constant Work
dB	decibel
DUT	Device Under Test
EG&G	Edgerton, Germeshausen & Grier
EO	Electro-Optic
EZ	Easy (brand name)
Hz	Hertz
InGaAs	Indium Gallium Arsenide
LASER	Light Amplification by Stimulated Emission of Radiation
LD	Laser Diode
PD	Photodiode
PID	Proportional Integral Differentiated
P-N	Positive-Negative
Qc	Quebec (province of)
R&D	Research & Development
Si	Silicon
V	Volts
W	Watts

LIST OF ANNEXES

PAGE

PREFACE

"Our present society is becoming more and more dependent on information, which we need to transmit, store and display. The eye, a visible light sensor, is one of the main conduits of information to the human brain. It is not surprising then that optical signals in the visible and near infrared are playing an increasingly important role in communications in our electronic world."[1]*

The advantages of optical radiation over conventional electrical communications networks are numerous. One of the first is the reduction in the size required for antennas by a factor of 100. This is extremely advantageous in space applications where size and weight are particularly critical. Furthermore, the frequency of optical electromagnetic radiation exceeds that of microwaves. This has for effect increased sensing precision or increased data rate for communications. Another advantage of optical radiation is that it is immune to interference by electromagnetic or radio frequencies. The first time these advantages were shown to make a commercial impact was in the area of long distance telecommunications where optical fiber losses as low as .2dB/km were observed. In this particular case, optical repeaters were only required every 100 km.[1]

* Numbers in brackets designate references at the end.

INTRODUCTION

Technical advancement of the laser diode has made many of the various optoelectronic systems practical and affordable. Understanding how these operate is of prime interest since we are concerned with characterizing (testing) semiconductor light sources as accurately as possible. As we will later see there are many parameters to be determined, but the one of greatest interest will be optical power.

The term "laser diode" denotes a device which uses a semiconductor p-n junction in a laser (Light Amplification by Stimulated Emission of Radiation) system. This semiconductor material contains atoms and molecules that possess internal energy. The value of this internal energy is restricted to specific discrete values or energy levels. Figure 1 illustrates the energy levels which the electrons, in a typical atom, may possess. Each electron will always be found in one of these allowed energy states. The transition of an electron from one energy level to another is made possible by the absorption or emission of light. Light is absorbed or emitted in individual units called photons. Each photon is an electromagnetic wave which has a specific wavelength, determined by the semiconductor material and travelling in a specific direction.[2]

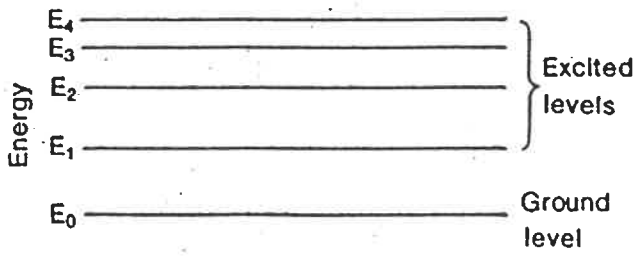

Figure 1. Energy Levels [2]

There are three types of electron transitions, as shown in figure 2. Firstly, figure 2a shows what is known as resonant absorption. An electron transits from the stable low energy level E_0, to the higher energy level E_1, through absorbing light. Secondly, figure 2b shows spontaneous emission. An electron transits from the high energy level, E_1, to the stabler low energy level, E_0. At the time, the energy balance of E_1-E_0 is released in the form of light. Since each electron, in the level, E_1, transits independently, light emitted is random and out of phase. Such light is referred to as incoherent and is a typical characteristic of spontaneous emission. In order to emit light, electrons must exist in E_1, with high probability, which is referred to as inversed population. Thirdly, figure 2c shows stimulated emission. The electrons in the higher energy level, E_1, are forcibly transferred to the lower energy level, E_0, by incident light. The light generated this time is referred to as stimulated emission light. Its phase is the same as that of incident light, because the stimulated emission light is emitted resonating to the incident light. Such stimulated emission is referred to as coherent light.

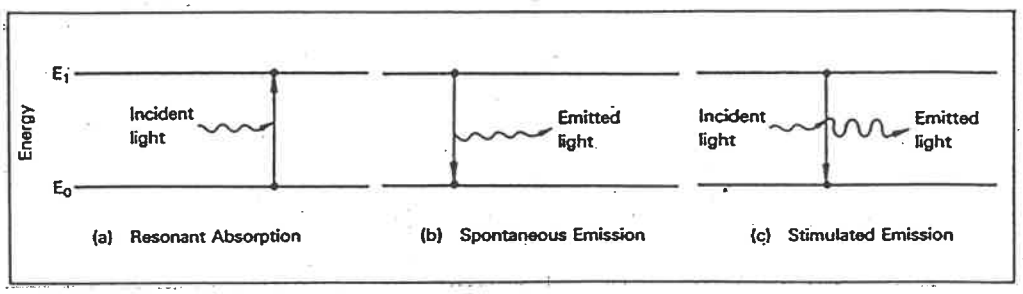

Figure 2. Transition Process [3]

Similarly to the electric circuit, laser oscillation requires the feedback function in addition to the gain which exceeds loss. Laser beams oscillate by amplification of stimulated emission and positive feedback with mirrors.

Figure 3 shows a Fabry-Perot resonator which is the most fundamental optical resonator. In forward bias (p -side +), electrons are injected across a P-N junction into the semiconductor to create light. Lasing is achieved by using the cleaved facets of the laser chips as mirrors and providing a waveguide

to confine light distribution. The stripe and heterojunction layers confine both the light and injected electrons to a small volume between the cleaved facets. When the applied current is increased enough, the hole and electron population are inverted. When this happens, the next electron injected creates a photon that traverses the cavity between the mirrors substantially amplified. The light emitted is of single energy (single wavelength) corresponding approximately to the bandgap energy of the semiconductor material.[4]

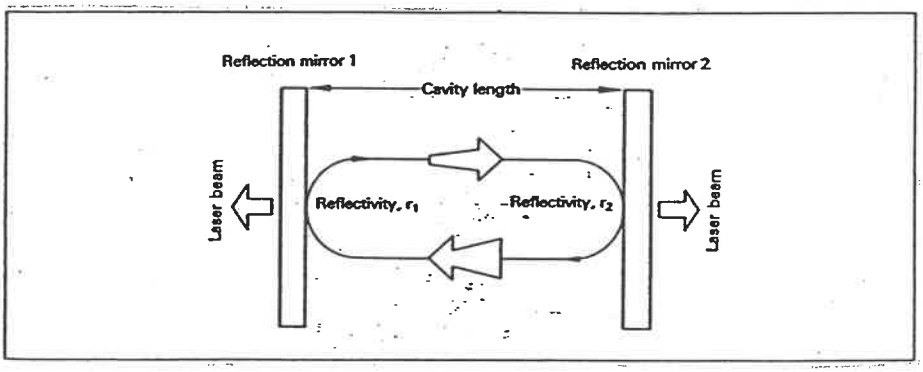

Figure 3. Fabry-Perot Resonator [4]

The light directed out of the mirror facet is not a pencil like beam, but rather a divergent elliptical source as seen in figure 4. This divergent elliptical source can be characterized by what the industry refers to as the perpendicular and parallel transverse modes, or more commonly the far-field. These semiconductor sources, being divergent, may be used in conjunction with lenses, to collect and direct as much light as possible. Given a certain application, customers will require a certain amount of light to be confined within a cone of specified angle, with its vertex at the emitting region of the laser diode. This is commonly referred to, in the industry, as the

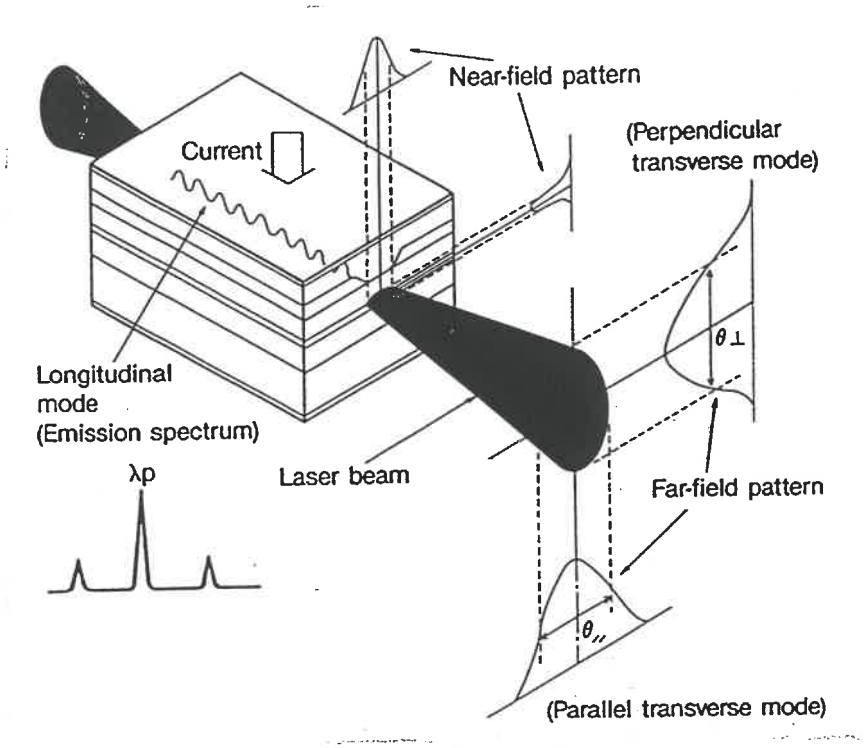

Figure 4. Laser Diode [5]

numerical aperture as seen in figure 5. It is then important to be not only able to measure all of the light emitted but to be able to determine what percentage can be found within a specified numerical aperture. There are many ways of controlling the parallel and perpendicular transverse modes of the emitting chip. These techniques are beyond the scope of this report and it will be sufficient to understand that different semiconductor sources emit in different transverse modes. Other factors that affect the farfield of a same device are electrical drive current, pulse width, and repetition rate, as well as device age and heatsink temperature. Figure 6 shows a chip mounted in what is commonly referred to as a CD (Compact Disc) package,

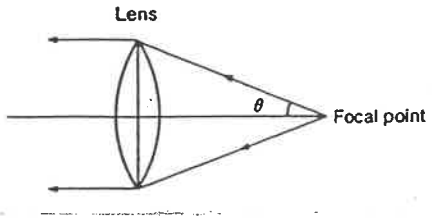

Figure 5. Numerical Aperture [6]

which is an industry standard, especially in Asian countries where many optoelectronic systems are assembled. EG&G Optoelectronics, in Vaudreuil, Qc, carries this package outline along with dozens of its own custom packages.

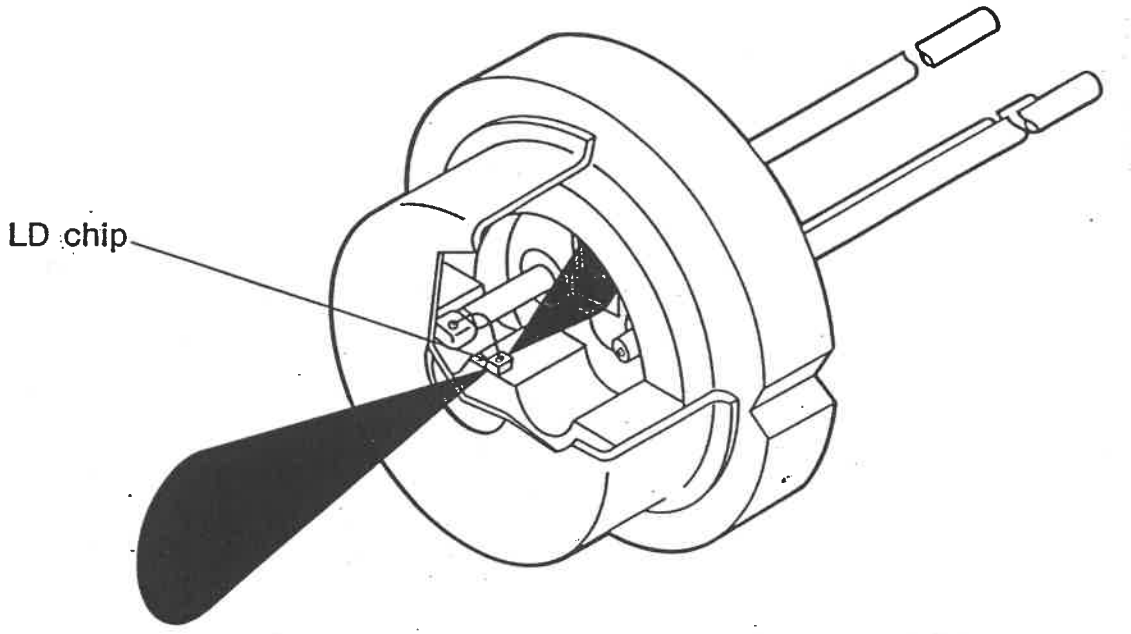

Figure 6. Laser Diode in a Compact Disc Package [7]

Some packages are customized exclusively to meet customer requirements, while others are designed for optimal performance of the laser diode chip. Furthermore, while some of the devices manufactured will operate at continuous currents (typically from 50mA to 200mA) many will require up

to 100 A pulsed at specific repetition rates (500 Hz to 20 kHz) and selected pulse widths (10 - 200 ns). Quasi-CW is a test condition that is seen more and more of as of late. Essentially a cross between the two aforementioned drive conditions, selected devices can be driven at pulse widths of 500ns to 10ms at repetition rates varying from single shots to 200 kHz and at drive currents ranging from 0 - 6 Amperes. What essentially limits the device drive current is its chip heat dissipation capabilities, which is often correlated against the duty cycle (percentage of time the device is being driven as a function of repetition rate and pulse width at a given drive current).

Knowing that the light emission is most importantly defined by the far-field (parallel and perpendicular transverse modes) and that this characteristic is dependent on drive current, heat dissipation, ambient temperature and age of the device, we must be able to quantify this particularity of the laser diode.

For many applications the measure of optical power into a numerical aperture is of greater importance than the total light emission. This is so because many optoelectronic systems are limited in their acceptance of light from divergent sources. That is to say that all light exceeding a given numerical aperture would be unusable and lost. By placing an aperture at a given distance from a laser diode,

one can measure the amount of light that is radiating through the previously defined aperture. On the other side of this aperture is a photodetector which essentially converts incident light flux into an electrical current. This electrical current would be a function of the wavelength and intensity of the incident light. But how does this photodetector operate?

> Photodiodes make use of a photovoltaic effect from application of voltage to both ends of a P-N junction at the time light exposes the junction. Under reverse voltage conditions at the P-N junction, a depletion region is generated to which an electric field has been applied as seen in figure 7. Incident light with the same energy as the bandgap energy is absorbed into the depletion region. The absorption of light produces electron-hole pairs. The electrons and holes then drift, under electric field action, in opposite directions across the depletion region. Electrons move forward to the cathode electrode, and holes move to the anode. As a result, a current flows through the load resistor and light signals are converted to electrical signals. Carriers produced in the depletion region are at high speeds due to acceleration by the electric field. Carriers generated in the diffusion region, however move slowly due to diffusion in accordance with the concentration gradients.[8]

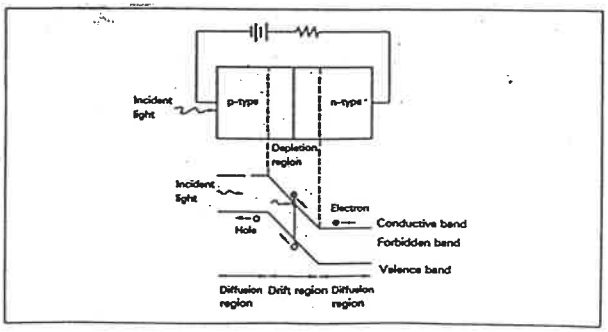

Figure 7. Photodetection Principles [8]

Figure 8 shows a typical set-up for characterizing optical power versus drive current of a LD (laser diode). Notice the absence of an aperture between the LD and PD (photodiode) which would yield "full collection" results. Tests at any numerical aperture are possible by placing a thin disk with the appropriate size hole at a calculated distance from the photodiode active area. The difficulties with these measurements on conventional set-ups such as that illustrated below will be discussed in the following chapters of the report.

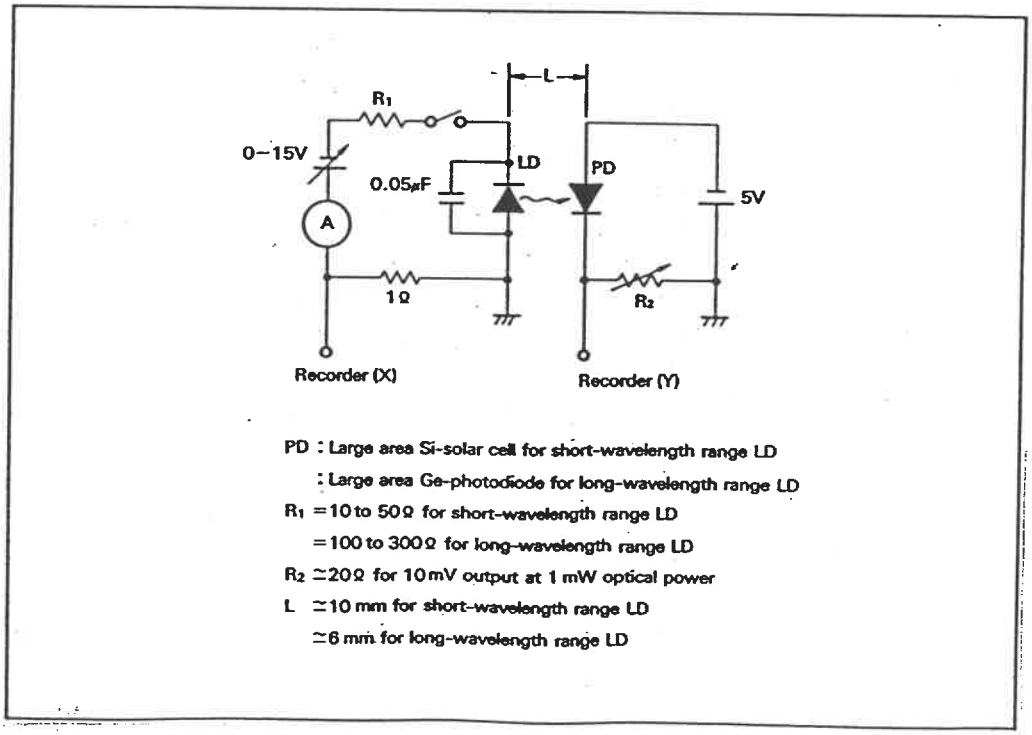

Figure 8. Conventional Optical Power Test Set [9]

INTEGRATING SPHERE THEORY

The throughput of an integrating sphere is defined as the ratio of light exiting a port to the total light entering its inlet port.

Note: The following equations are proposed by the sphere manufacturer, Labsphere Inc.

$$\phi_e/\phi_i = \frac{p * f_e}{1 - p * (1-f_j)} \qquad \text{Eqn 1}$$

where ϕ_e = total light exiting a port in Watts

ϕ_i = total light entering a port in Watts

f_e = area of exit port/surface area of sphere

f_j = sum of all port areas/surface area of sphere

p = sphere wall reflectance (dimensionless)

It should be mentioned that equation 1 is only valid when the light is incident on the sphere wall and the reflectance of all ports is zero, as shown in figure 9.

The exit port radiance is given by

$$L_s = L_e = \phi_e / (\pi * A_e) \quad \text{in Watts/ m}^2 \qquad \text{Eqn 2}$$

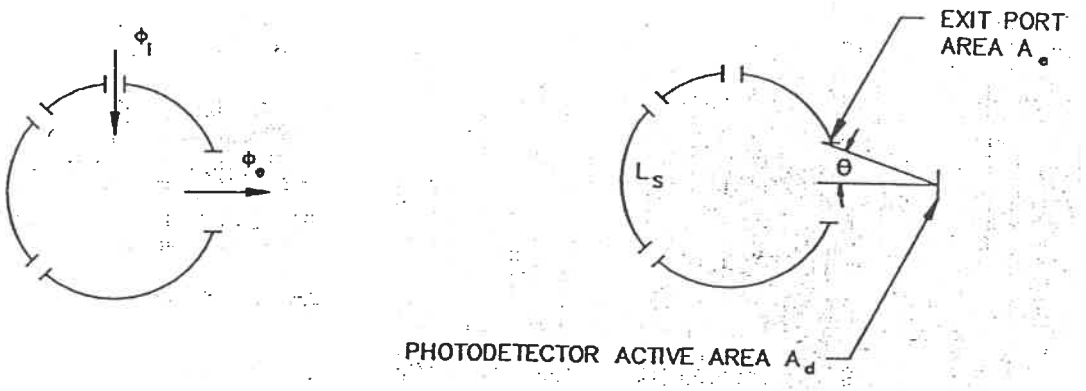

Figure 9. Basic Integrating Sphere

where L_e = exit port radiance in Watts/m²

L_s = sphere wall radiance in Watts/m²

A_e = exit port area in m²

Combining equations 1 and 2 yields

$$L_s = \frac{p * \phi_i}{\pi * A_s * (1-p*(1-f_j))} \quad W/m^2 \qquad \text{Eqn 3}$$

The total flux incident on a detector active area is defined as follows:

$$\phi_d = L_s * A_d * \Omega \text{ in Watts} \qquad \text{Eqn 4}$$

where A_d = active area of photodetector in m²

Ω = projected solid angle (dimensionless)

where $\Omega = \pi * \sin(\theta)^2$ for $A_d << A_e$ Eqn 5

Having all the equations necessary to determine the amount of light incident on the active area of the detector we can now proceed to a calculation.

For the sake of comparison the actual dimensions and characteristics of the EG&G prototype sphere will be used.

$p = .993$

$r_i = 3.17$ mm (radius of inlet port at sphere inner skin)
$r_e = 7.54$ mm (radius of outlet port at sphere inner skin)
$r_s = 29.81$ mm (radius of sphere taken at the inner skin)

$A_s = 4\pi r_s^2 = 11\ 174\ mm^2$ Eqn 6
$f_j = \pi * (r_i^2 + r_e^2) / A_s = .0188$ Eqn 7
$A_d = .786\ mm^2$ (detector active area)

$\Theta = 33.6°$
$\Omega = \pi * \sin(\Theta)^2 = .962$

$A_d/A_e = .786/(\pi * 7.54^2) = 4.4 \times 10^{-3}$

Since $A_d << A_e$, the manufacturer's equations can be used.

Combining equations 3 & 4 we obtain the following

$$\phi_d/\phi_i = \frac{p * A_d * \Omega}{\pi * A_s * (1 - p * (1-f_j))} \qquad \text{Eqn 8}$$

$$= \frac{.993 * .786 * .962}{\pi * 11\ 174 * (1 - .993 * (1-.0188))}$$

$$= 8.33 \text{ X } 10^{-4}$$

Actual throughput values were measured to be $8.05 \text{ X}10^{-4}$.

$$\text{Percent Difference} = \frac{\text{Theoretical - Actual}}{\text{Theoretical}} \text{ X } 100$$

$$= \frac{8.33 \text{ X } 10^{-4} - 8.05 \text{ X } 10^{-4}}{8.33 \text{ X } 10^{-4}} \text{ X } 100$$

$$= 3.4\%$$

Note: Refer to the experiment on integrating sphere throughputs, in Annex 4, for actual throughput measurements.

CHAPTER 2

TECHNICAL SIGNIFICANCE

Measuring optical power emitted from LDs (laser diodes) has long been done with photodetectors calibrated for that purpose. Several problems are typically encountered when one of these LDs is placed directly in front of a photodetector to capture the light emitted.

The first and without any doubt a very disturbing problem is saturation. Photodetectors can convert only a maximum quantity of light into electrical current linearly. If this amount is exceeded, the electrical current generated by the photodetector will not correlate to the correct optical power, calculated from a calibration factor established within the photodetector linear range. In effect, at some point, doubling the optical power incident on the photodetector will not double its electrical output.

Using an optical filter, of known attenuation, between the LD source and the photodetector may solve the saturation problem but creates another problem of choice. Optical filters show undesirable properties such as reflectivity. Ideally, filters should be purely attenuating. By not having this exclusivity, it becomes difficult to believe in a filter calibration since LDs have emissions that strike a surface at different angles. The angle at which the light

strikes a surface will often determine if it is refracted or reflected.

The third problem encountered with a simple LD - PD arrangement is that LDs have divergent emissions which cannot be completely captured by photodetectors of finite dimensions. One would be inclined to think that simply approaching the LD source to the photodetector active area would solve this problem. This is not so for the following reason: approaching the light source too close to the photodetector would result in localized saturation on the active area of the photodetector. Making the photodetector very large as to be able to distance the source and the detector is not a cost effective manufacturing practice. Furthermore, the response times of large area photodetectors are poor and not well suited for narrow optical light sources.

It is understood how the addition of an integrating sphere between the source (LD) and the PD alleviates these problems.

The integration sphere, used at EG&G, is essentially hollow with highly reflective coating on the inside. Two

half inch ports, 90° apart, are located on the skin of this sphere. The first port will be deemed the inlet for the source while the other will be for the photodetector. An additional port was installed so that an attached fiber bundle exiting to a spectrometer could be used to perform spectral analysis at the same time optical power measurements are being made.

Only a fraction of the light emitted from the source into the sphere will be incident on the photodetector, reducing the risk of saturation. Should a saturation problem be anticipated, the fraction of light incident on the photodetector can be further reduced by placing a longer extension tube between the photodetector and the exit port. It is then possible to avoid saturation problems by using the integrating sphere in conjunction with exit port extension tubes. The goal to perform "full collection" measurements, on the conventional optical power test bench, is what in many cases lead to saturation problems and the need for optical filters. By placing the light source emitting chip flush with the integrating sphere inner skin, full collection measurements are guaranteed regardless of the divergence or orientation of the beam, by the very principle of the integrating sphere.

The conventional optical power test bench with its filters, apertures and photodetectors is known to attenuate the light before converting it into an electrical current. The intention is to attenuate this light by a known percentage but the components behave less than ideally and the result is a calibration factor which is sensitive to light divergence, intensity and orientation. The integrating sphere, along with the attached photodetectors and extension tubes, has a tremendous advantage over conventional set-ups since it consistently samples a known percentage of light without the problems of conventional optical power test benches.

CHAPTER 3

DESIGN CONCEPTS

When it was first decided that the prototype sphere had to leave the applications laboratory, to be introduced into the manufacturing area, several concerns were voiced. Many of these concerns had to do with the feasibility of taking away this "high-tech toy" from a qualified technician and giving it to an operator with relatively no training, no technical studies and no feel for the integrating sphere operating principles. Many wondered if the same accuracy and repeatability of measurements could be expected once the integrating sphere was transferred to the manufacturing area. For the above reasons, management and marketing found it necessary, and justifiably so, to draw-up a clear mandate for the individual or individuals who would be made responsible for the inclusion of the integrating sphere test station into the manufacturing area.

3.1 MANDATE

The original mandate specifying the integrating sphere test station simply stipulates the following: the test station must be capable of testing all devices regardless of their package style, test temperatures, drive currents or cone angle measurements required. Minimum set-up time must be required by the manufacturing supervisor so that the

supervisor will prefer this test station over others. An operator with little training and no technical background must be able to perform these tests accurately and without constant supervision.

Ensuring that the layout of this test station stays true to the original mandate turns out to be extremely labor intensive for the following reasons: optical power measurement test benches are not stock or even standard items. Most users customize their own or pay dearly to have them customized. To complicate matters, the conventional photodetector and filters are being replaced by a bulkier integrating sphere with accessories of its own. High current pulse drivers have to be incorporated into this test bench with electrical inductance being one of the main concerns. A method of cooling and heating devices from -55°C to 125°C has to be devised and incorporated into this test bench. Many package styles exist and it is important to locate the point of light emission for each of these devices undergoing optical tests, while maintaining proper heatsinking. Rigidity is of prime concern since alignment errors in the X,Y,or Z planes or orientation errors lead to erroneous optical power readings. Hence, there are a lot of considerations.

3.2 MECHANICAL LAY-OUT

With so many constraints it is difficult to determine where to start designing this station. The most logical approach is to build around the DUT (Device Under Test), since the final product is always of greater interest than any fixturing or test equipment.

The DUT is held in a fixture to ensure proper alignment and orientation as well as providing adequate heatsinking. Directly behind this device holder is an area reserved for electrical connections. In many cases, where CW (constant work) or QUASI-CW measurements are made, simple clips can be hooked-up to the terminals of the DUT with the electrical driver (current source) some convenient distance away. However when high current (30 Amperes or more) and narrow pulse width (100ns or less), conditions are required, the termination box of the high current supply must be as close as possible to the electrical terminals of the DUT to reduce inductance, permitting smaller pulse widths and higher currents. A 3-axis dovetail slide arrangement is provided to accurately align the termination box electrical terminals with those of the DUT. Figure 10 shows the mechanical lay-out of this optical power test station.

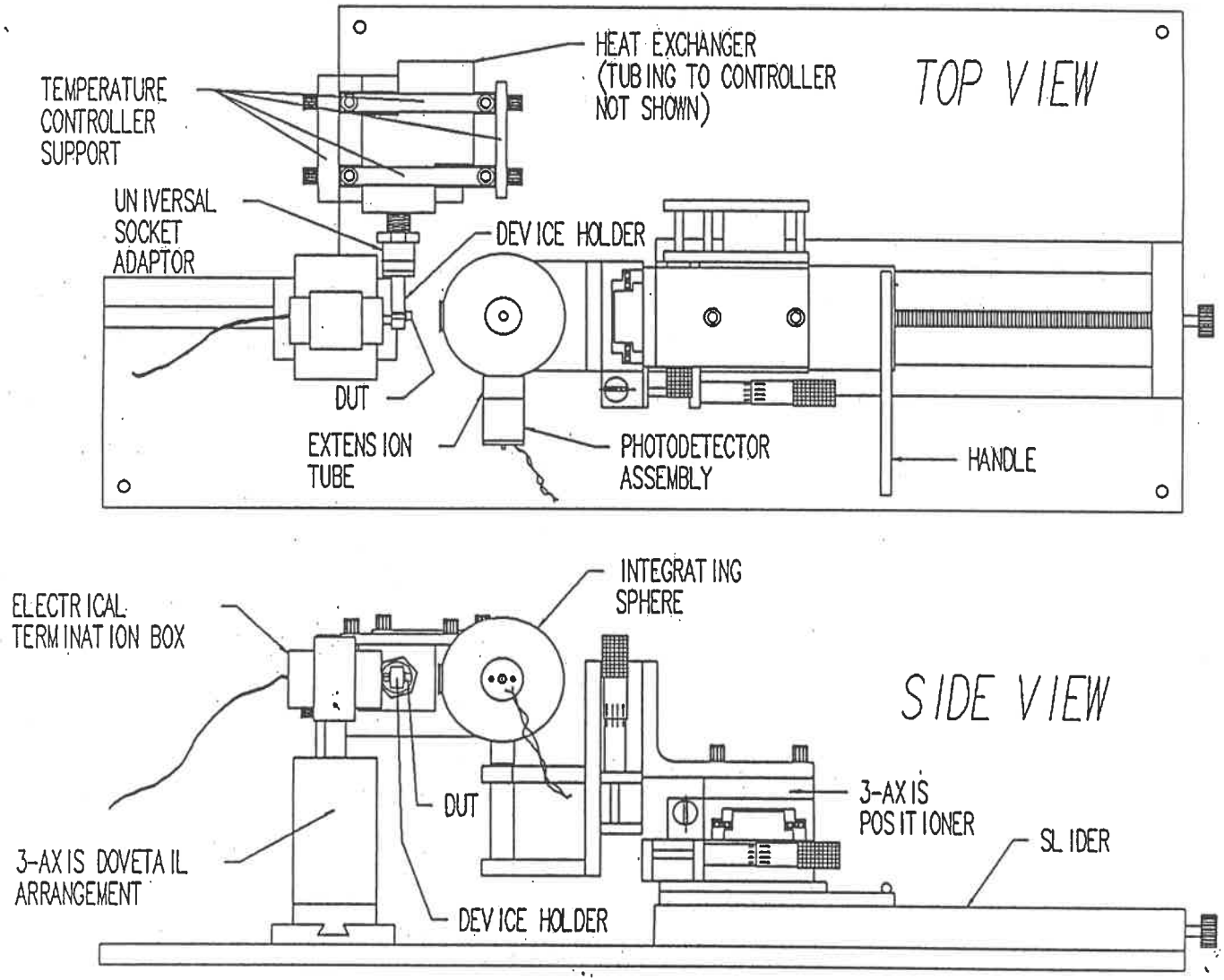

Figure 10. Integrating Sphere Optical Power Test Station

Directly in front of the DUT is an area non-obstructed and reserved for the integrating sphere. This area needs to be free of obstructions for several reasons. The first reason is that "full collection" measurements are made with the emitting region of the device flush to the sphere inner skin. For this to be possible, the DUT must be allowed to nest into the inlet port of the sphere. The second reason is that devices need to be removed and inserted from this area to be tested. Clear access makes this operation safer and faster for the operator. With the use of custom fixturing, the integrating sphere is solidly mounted on a 3-axis positioner. This manipulator allows the position of the sphere inlet port to be properly aligned and centered flush to the emitting region of the device. This is verified with the use of an alignment fixture and is then referenced as (0,0,0) in the X,Y,Z coordinate system. Proper orientation of the sphere (angular alignment) is done by rotating the sphere about its support until the face of the inlet port is parallel to the face of an alignment fixture provided for that purpose. The support is then secured by tightening the slotted hole it rests in. The 3-axis manipulator, holding the sphere, is secured to a slider which in turn is secured to a baseplate. This slider, which permits displacements along the principal axis of light

emission, has two functions. The first function of the slider is to disengage the sphere after a test has been completed so that the device can be removed and another one inserted. Its second function is to measure and set a distance corresponding to a specified numerical aperture. Light emissions radiating into an aperture of fixed diameter at a given distance quantifies what the industry refers to as cone angle measurements. The operational procedure, in annex 3, explains how these cone angle measurements are made.

A temperature controller, capable of -55 to 250 °C, has custom fixturing attached to its probe so that devices can be heatsunk during optical tests while being held rigidly in a referenced point in space. Annex 5 quantifies the thermal performance of these fixtures interacting with the temperature controller. Finally, the area nearest to the operator is kept free of obstructions for easy access to all areas (i.e. current drivers, device holders, slider etc.). All efforts were made to keep this station compact to minimize cost and maximize ergonomics.

The integrating sphere test station shown in figure 10 is the result of a prototype redesign (i.e. 2nd generation).

The mechanical layout is essentially the same as the first generation except that the temperature controller is more performant allowing minimum device temperatures of -55°C whereas the first generation test bench was limited to -46°C. The 3-axis positioner was replaced by a sturdier one whose manipulators are now tucked away on the sides of the stages to prevent these from being perceived as handles, by the operator. The fixtures that secure the sphere to the positioner have also been made sturdier to ensure the required rigidity. The biggest change, however, is the device fixturing. First generation fixturing was only partially successful in meeting the mandate. The short comings of the first generation device fixtures will be further discussed later. In brief, the second generation lay-out saw some welcome changes including better designed device holders, sturdier mechanical components as well as proper calibration procedures for the production supervisor and operational procedures for the operators.

3.3 ELECTRICAL DRIVERS

The electro-optics industry counts three different electrical test conditions; CW (constant work), Quasi-CW and pulsed. Fortunately, this is one area where intensive

design effort was not required.

3.3.1 Constant Work

Many drivers of excellent quality are commercially available. There was really no engineering or financial justification to design one of our own. A simple transient free, current source (0 - 500mA capability) was chosen for its performance to cost ratio and adopted not only for the integrating sphere test station but for all test stations requiring constant current drive conditions. Electrical patchcords running from the positive and negative terminals of the supply to the device provide the required electrical bias. Figure 11 shows a typical CW current driver recommended by a world reknown supplier of optoelectronics devices.

3.3.2 Quasi-CW

The quasi-cw driver was assembled at EG&G Optoelectronics, in Vaudreuil, Qc. Its components were chosen to power devices at several millisecond pulse widths at arbitrary repetition rates (up to 200 kHz) and currents ranging from 0 to 6 Amps. A typical quasi-cw drive setting

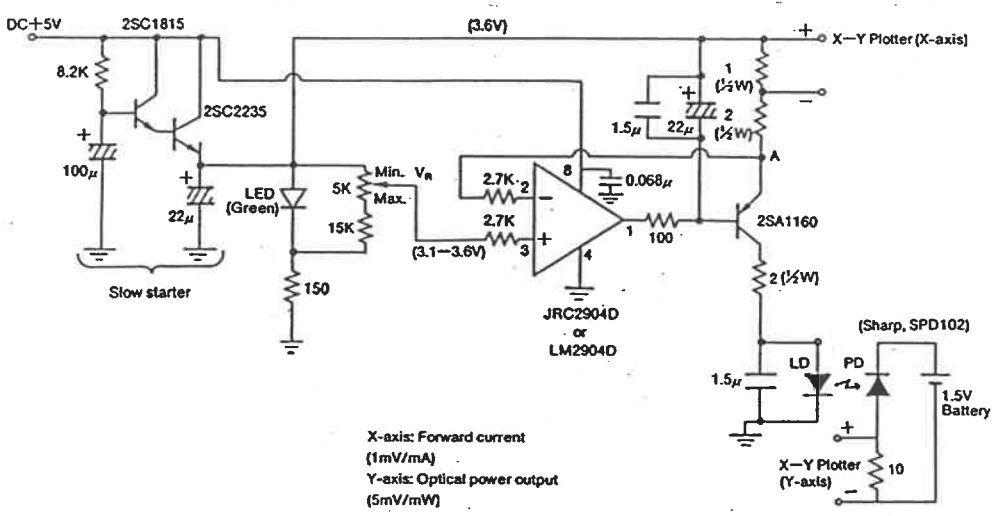

Figure 11. Typical CW Driver [11]

would be 1 millisecond pulse width, repetition rate of 100 Hz and a current of 2 A. Again electrical patchcords from the positive and negative outputs of the current driver supply the DUT with the required electrical bias. Figure 12 shows the quasi-cw circuit along with application notes.

3.3.3 Pulsed

The greater part of the devices tested on the integrating sphere will be under "pulsed conditions". When the term "pulsed" comes into discussion, it is understood that the drive current is typically anywhere from 10A to 100A at repetition rates varying from .5kHz to 12kHz at very

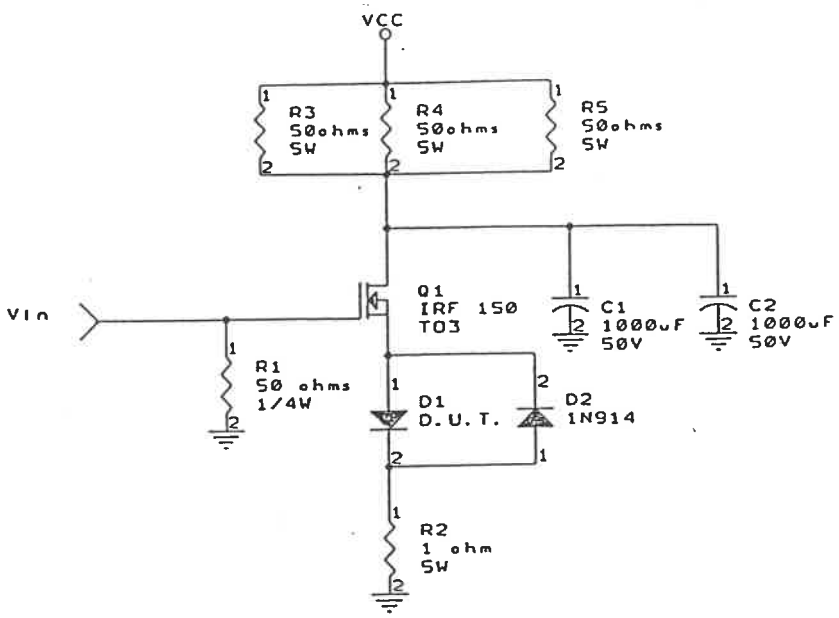

NOTES

1. The combination of R_3, R_4, R_5 and C_1, C_2 determine the maximum frequency of operation.
2. Peak forward current is monitored across R_2.
3. The locations of D_1, D_2 may be interchanged with Q_1 and the value of R_2 may be reduced for higher current applications
4. V_{in} is a positive pulse which provides I_f and repetition rate control.
5. The following drive conditions are possible but not necessarily simultaneously

I_f: 0 - 6 Amps
Rate: single shot to 200 KHz
Pulse width: 500ns to 10ms

Figure 12. Quasi-CW Driver

narrow pulse widths (10-200ns). Again, fortunately, these kind of drivers are commercially available where repetition rates, pulse widths and drive currents are all individually adjustable. These pulsers have one drawback however. They require special fixturing. The current travels down a double copper strip-line separated by an electrically

shunting material. It became part of the design exercise to terminate this strip-line with something which lended itself more easily to biasing devices with one or more .5mm diameter leads. A small enclosure approximately 75mm long by 50mm wide by 50mm deep was used, as the termination box. The strip line is soldered into a male D-connector assembly. The corresponding female connector is fixed to the outside of the termination box where its inside terminals are connected to an electric circuit board. This circuit board holds low inductance resistors to match the impedance of the strip line to the termination box, limiting undesirable electrical ringing effects. Protection diodes are also present to protect the DUT from being damaged in the eventuality of a reverse voltage spike. Finally, at the other end of the termination box, two solder terminal have been installed to accept the leads of the device to be tested. Two different termination boxes were assembled as shown in figure 13. One rated up to 50A for the narrower pulse widths (80ns +) and one rated up to 100A for the larger pulse widths (120ns +). An increase in the minimum pulse width is never desirable, but in the case of the 100A termination box the extra resistors required increased the inductance and capacitance of the circuit, which inherently raised the minimum pulse width allowable.

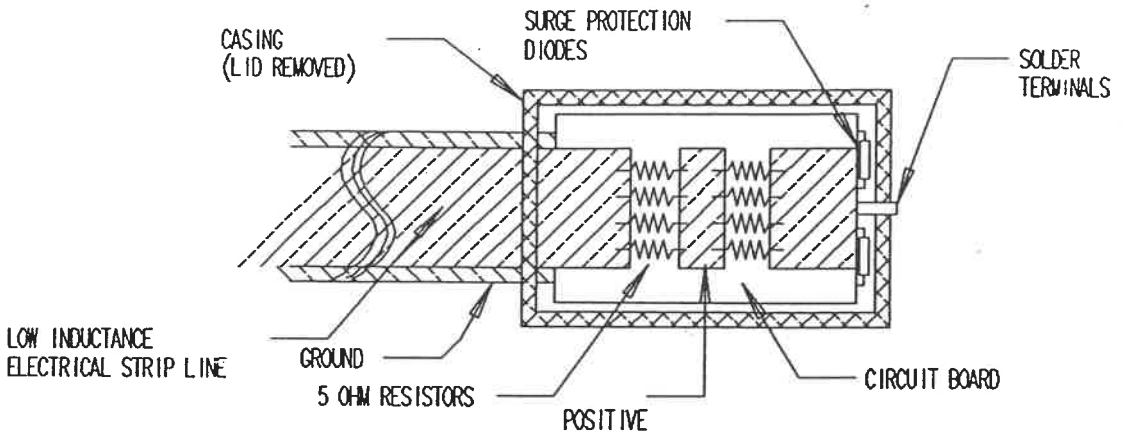

(a) RATED 100 Amps

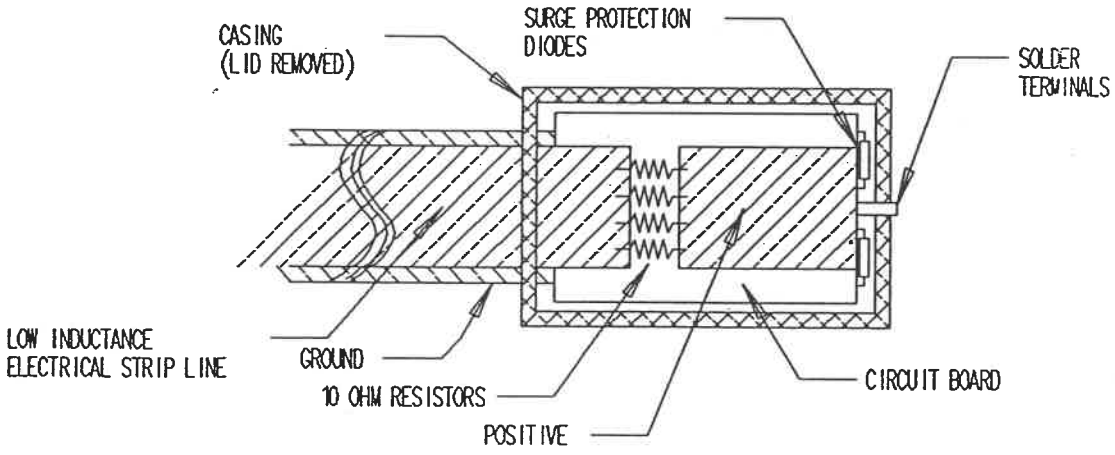

(b) RATED 50 Amps

Figure 13. Pulsed Driver Electrical Termination Boxes

3.4 THERMAL CONSIDERATIONS

The need to test devices at temperatures ranging from -55 to 125°C creates a problem of choice. Somehow the device fixtures must mate into a unit capable of cooling and heating. This same unit has to be able to stabilize the device holder to a selected temperature. -55°C is not a temperature that is easily reached, when considering the convective losses with the environment. The reader is reminded that the difference between standard room temperature (25°C) and -55°C is greater than that of standard room temperature and the boiling point of water. Furthermore, cooling is an extremely inefficient process compared to heating. Upon evaluating several temperature controllers, with appropriate fixtures, it was found that only one could achieve -55°C. The temperature controller ,with the two stage compressor, pumping refrigerated freon to a metal heatsink, via flexible conduits, proved to be the best choice. This same metal plate has heating elements as well as a thermocouple attached to it. The whole assembly is encased in plastic with a stainless steel 9/16-18, 18mm long, threaded stud protruding. This stud is used as the conducting element for heat exchange. The temperature logic controller, continually monitoring the thermocouple,

regulates the heating elements and the flow of cooling fluid. The controller has temperature settings accurate to .1°C as well as user programmed temperature settings. The compactness of the plastic encased metal plate also makes this system a favorite considering the need to keep thermal masses to a minimum allowing higher device temperature extremes and quicker settling times. This temperature controller can stabilize a device to from 25 to -55°C in less than 7 minutes or to 85°C in less than two minutes.

N.B. A thorough thermal analysis of the performance of this temperature controller in conjunction with the custom device holders, designed at EG&G, is presented in Annex 5.

3.5 OPTICAL ACCESSORIES

As mentioned earlier, the traditional photodetector with attenuator and superimposed aperture is being replaced by the integrating sphere, a photodetector assembly and other accessories. The integrating sphere has its inlet port at 90° to its outlet port. Both of these ports are at 90° with the vertical post supporting the sphere. Highly reflective packed powder is used on the inside of the sphere. Attached to the inlet port is a defining aperture.

The device to be tested is not placed flush with the inlet port, but at the sphere inner skin for full collection measurements. All photodetectors are mounted in custom housings. These photodetector assemblies, whose insides reveal low pass electronic filters, are then mounted on the sphere outlet port. Two terminal leads to reverse bias the photodetector and a photodetector output coaxial cable are located on the back of this photodetector assembly as shown in figure 14.

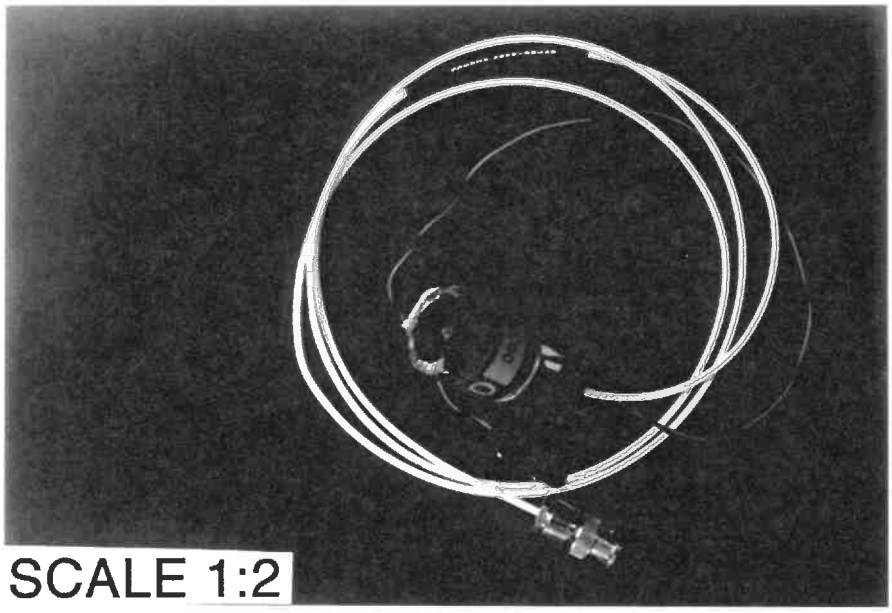

Figure 14 Photodetector Assembly

The traditional photodetector is not being replaced. It is the attenuating filter that is being replaced by the integrating sphere and its exit port extension tubes. The

integrating sphere not only acts as a diffuser supplying light of Lambertian (random) form but by its detector port area to sphere inner surface area ratio allows only a certain percentage of the light to become incident on the photodetector. This percentage can be further reduced by placing an extension tube between the outlet port and the photodetector assembly. Naturally, calibration data is made available to the user referencing the integrating sphere serial number, photodetector serial number, extension tube length and wavelength of interest.

3.6 DEVICE FIXTURING

When the specification for the integrating sphere test station was first drawn-up, it became obvious that some of the devices that required testing had never been tested before. It becomes not only a task of adapting and improving the test fixtures from other optical power test stations, but completely rethinking the way some of these devices are to be tested. Many different problems have to be solved in order for this design effort to be viewed as a success. First and foremost, the device holder has to be able to hold the DUT in a fixed position (X,Y,Z) and orientation. The device holder also has to provide adequate

heatsinking so that temperature fluctuations are kept to a minimum at either extreme (-55 and 125°C). They must allow for their temperatures to be monitored and they must be easy to install into the socket of the temperature controller, regardless of the package type they are accommodating. The thermal mass and convective areas must be kept in consideration such that the required device temperature extremes of -55°C and 125°C can be met. Another requirement for the device holder is the need to connect the electrical terminals of the device to the current driver. The test station must be able to accept many device holders without any long set-ups. Furthermore, the geometry of the fixtures must be such that they do not restrict the movement of the sphere. Loading and unloading times must be kept to a minimum for reasons that don't need to be explained in a manufacturing environment. The ability to verify the positional alignment and orientation of the fixture is also important.

Resorting to the "divide and conquer" philosophy proves to be effective in completing this difficult task. The fixtures are quickly divided into three subgroups: universal socket, device holders and alignment fixtures.

3.6.1 Universal Socket

The universal socket is essentially the interface between the temperature controller and the device holders.

Our first attempt at making the universal socket is only partially successful. The design is simple, perhaps too simple. Figure 15a shows the 1st generation universal socket design. The device holder end is rectangular in cross section with a hole drilled in its side. The universal socket, essentially a square hole cut into a brass piece ,also has a hole through its side. A dowel is inserted from one side of the universal socket through the device holder side and finally out the other side of the universal socket. The universal socket has a female thread machined on one end to match the male thread on the temperature controller probe. The threaded brass piece is separated from the square holed brass piece by a metallized ceramic. This ceramic provides the necessary electrical shunt while maintaining good heat dissipation capabilities between the device holder and the temperature controller probe. This ceramic component was necessary due to the fact that several devices tested have their case electrically shorted to their positive terminal and the temperature

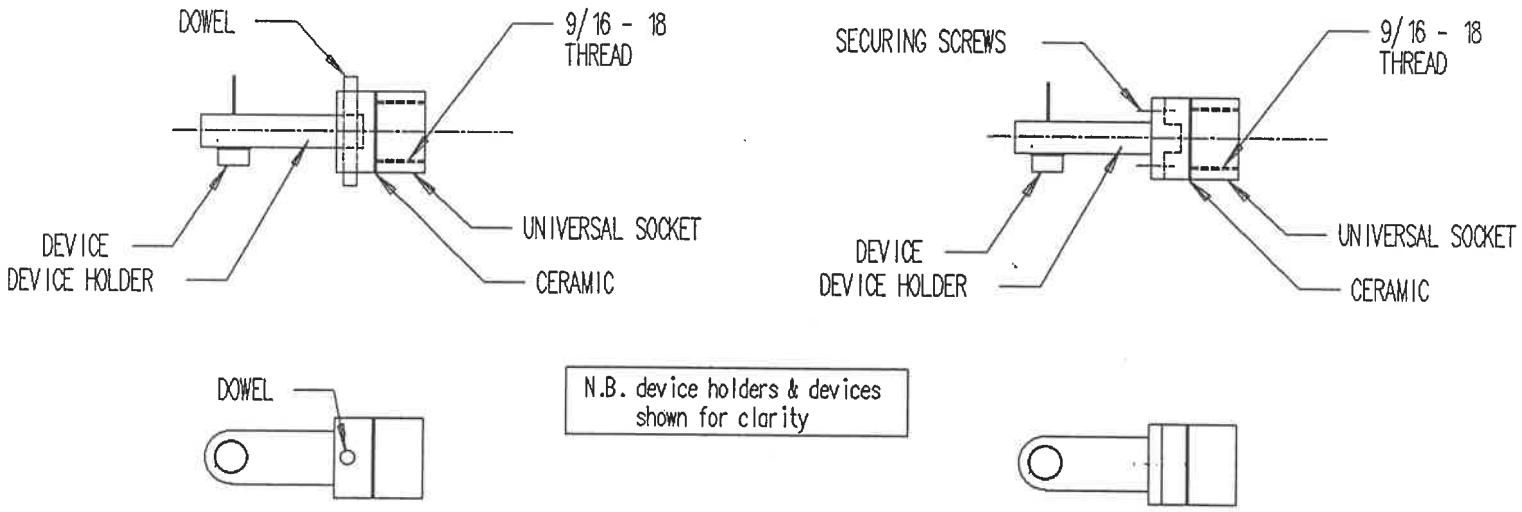

Figure 15 Universal Socket Assemblies

controller probe is connected to ground. This effectively would have meant an electrical short to ground, making biasing case positive LDs impossible. In the aftermath, the following came out. The use of the ceramic, as an electrical shunt and thermally conductive material, was a success. The universal socket was of small enough size as to limit heat losses to the environment. The materials that were chosen performed well after endless hours of use and repeated temperature cycling. Unfortunately, it was discovered that the device holders wobbled in the universal socket due to too much clearance between the mating parts. These excessive clearances cause errors in alignment and device holder orientation. The poor contact between heat exchanging surfaces is also limiting temperature extremes that the device holders can be cycled to.

Our second attempt at the universal socket keeps the same approach at the temperature controller end but changes drastically at the interface between the device holder and the universal socket. It is quickly understood that locating the device holders accurately and consistently requires more than a dowel insert. The dowel insert approach is not at fault, in the previous design, but rather he machining tolerances that cannot be kept tight enough.

These under specified tolerances cause the "sloppiness". Instead of using a square hole, a round one is counterbored down the center of the universal socket as shown in figure 16. The device holder end is obviously a cylinder of similar depth and diameter. The device holder has flanges with through holes for the same size screws as those tapped in the universal socket face as shown in figure 15b. What results is an assembly that relies on few dimensions and tolerances to assure a good mate every time. Furthermore,

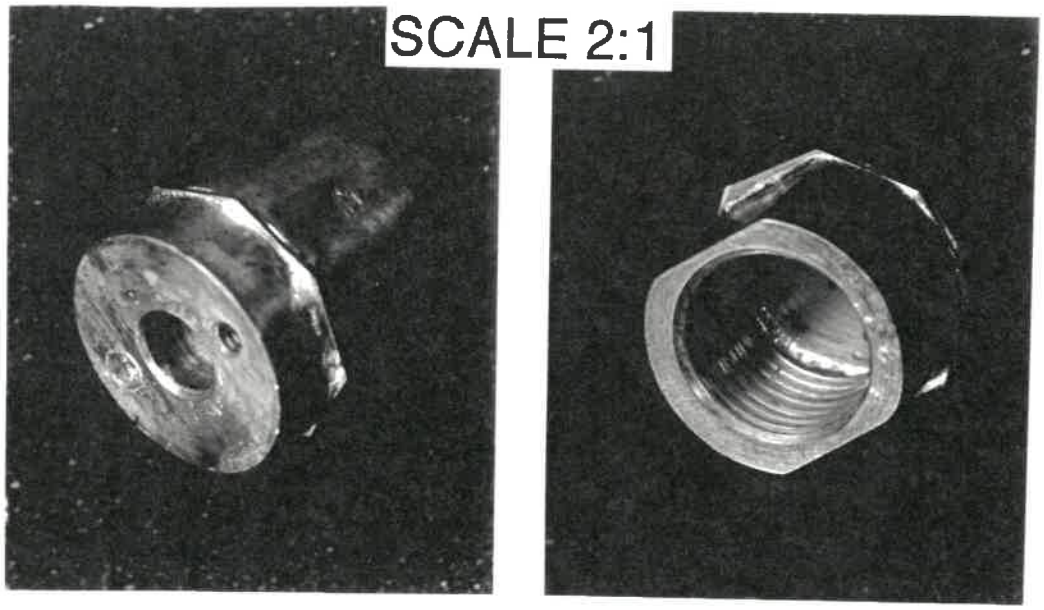

Figure 16. Universal Socket

the presence of screws assures a better thermal contact between heat exchanging surfaces, reducing thermal resistance and hence increasing possible device temperature extremes. Thermal grease is still used between all mating surfaces, as long as there is no chance of contaminating the DUT. It is then understood how the redesign of the universal socket has helped achieve the required positional and thermal stability required while still maintaining an easily machinable specification.

3.6.2 Device Holders

The second item of interest in this group is the device holder. We can classify the product tested, at EG&G, on this station into three categories: coaxial studs, transistor outline and substrates devices.

3.6.2.1 Coaxial Stud Devices

The coaxial stud devices are the easiest to design device holders for. In effect, these devices, as the name implies, have a lead, usually for positive bias, coming down the center of the package electrically isolated from the case by a glass sleeve as shown in figure 17. The case of

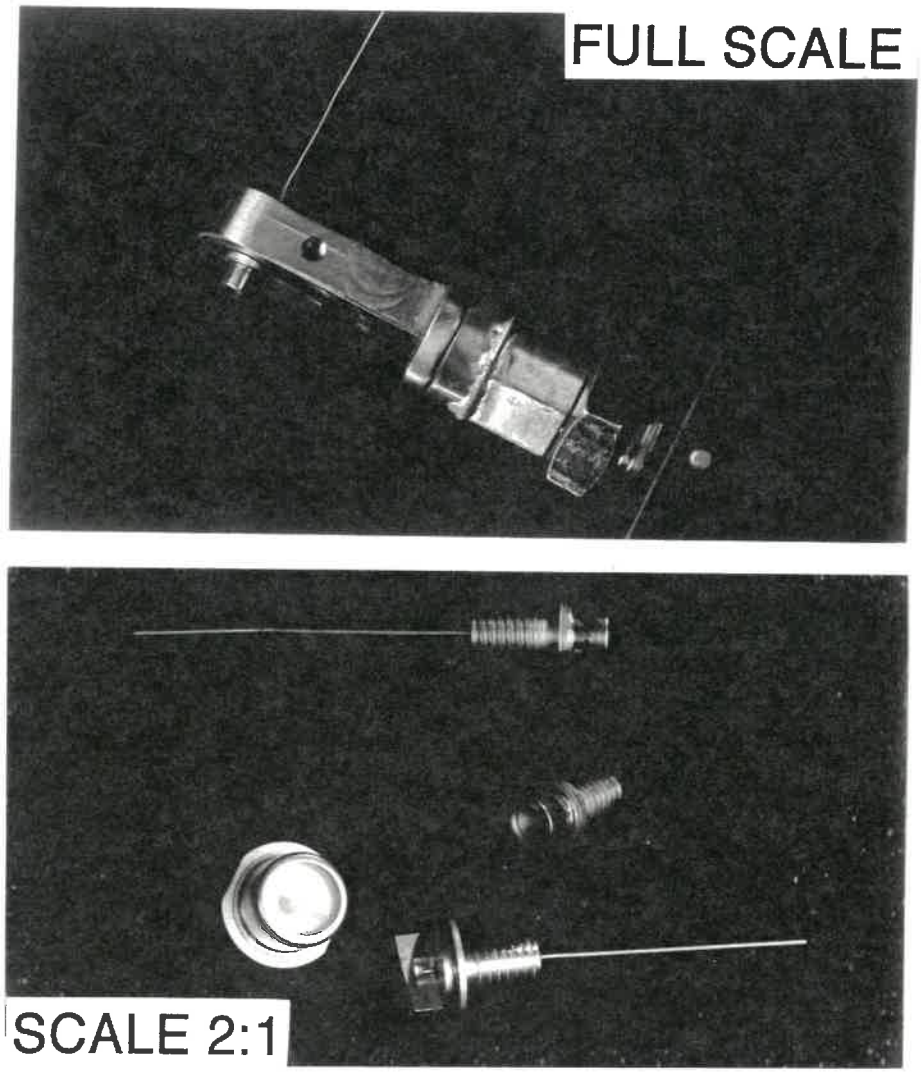

Figure 17. Coaxial Stud Holder (top) and Devices (bottom)

the device, usually made of stainless steel or copper - tungsten, will be the other electrical lead. A male screw thread is located on the back of these devices. This makes securing these devices onto a heat sink extremely easy. Since the shoulder of the device rests squarely on the device holder, one needs only to assure that the normal axis of the device holder is pointing in the right direction to guarantee the same orientation and position of the DUT every

time. In brief, the heat sinking capabilities of these device holders as well as their orientation and alignment repeatability is excellent.

3.6.2.2 Transistor Outline Devices

Transistor outline devices are somewhat more difficult to design device holders for. The devices they accommodate don't have the practical screw feature of the coaxial stud device. Instead, this device holder relies on an plastic sleeve to press down the flange of the device onto the heat sinking surface. The labor required in testing a batch of 100 of these devices is twice that of testing the same quantity of coaxial stud devices because of the extra part that needs to be handled (i.e. the sleeve). The sleeve thickness is such that the light emissions from the device will not be clipped by it. Figure 18 shows a transistor outline device in this device holder.

3.6.2.3 Substrates Devices

The substrate device holder is definitely the hardest test fixture to design. Difficulties arise due to the fact that these devices are small, fragile and worst of all have

no electrical leads protruding. Like the transistor outline device, the substrate device is difficult to orient and position. Unlike all other devices, substrate devices have to be probed to be biased electrically. Some of the substrate devices tested at EG&G Optoelectronics, Vaudreuil, Qc, are as small as 2.5mm by 1.25mm by .3mm thick as shown in figure 19. The probes have to be at least 1.75mm apart in order to avoid shorts and arcing.

The design of the substrate device holder is as follows. As shown in figure 20 the device is nested into a brass fixture which mates with the universal socket. The brass

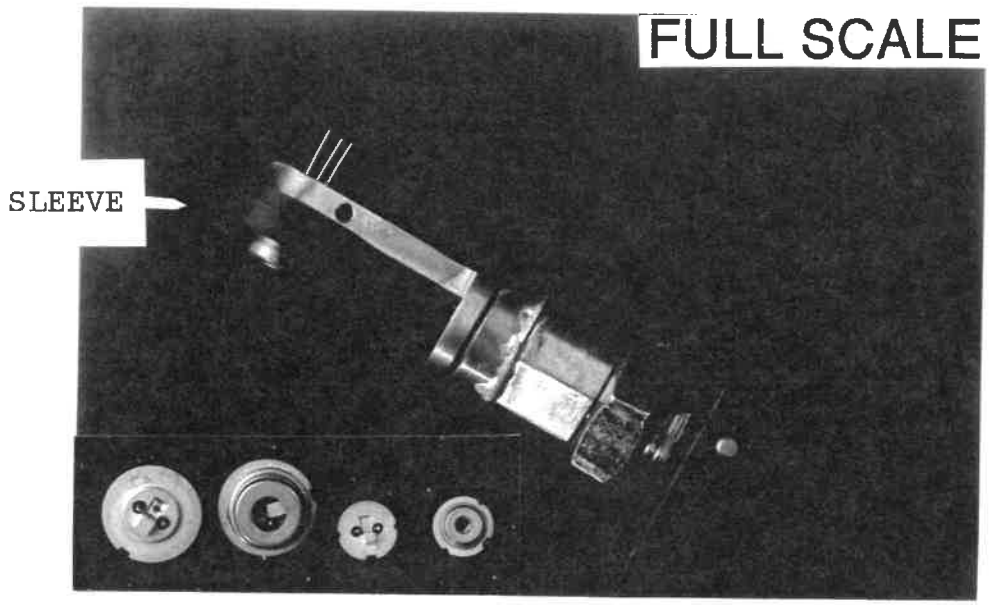

Figure 18. Transistor Outline Device Holder and Devices

fixture is designed as to ensure that the edge of the substrate device is flush with its edge, facing the sphere inlet port. Two guide posts are screwed in vertically into the brass fixture to allow an electrically insulating block of material to position and secure two spring loaded probes.

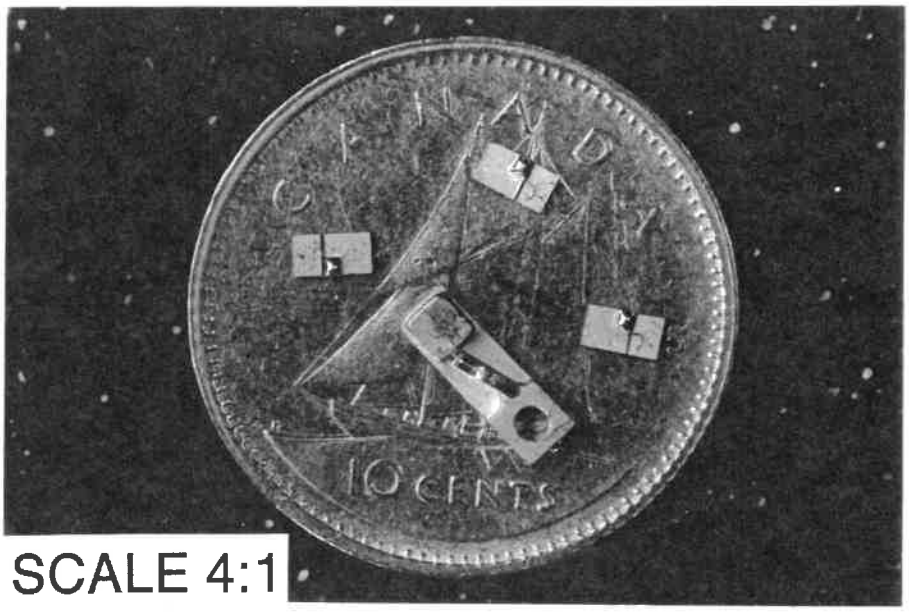

Figure 19. Substrate Devices

The probes, themselves nested in gold plated solderable sockets, have limited travel (as little as 1.75mm), and rely on the vertical motion of this block to engage and disengage the DUT. The guide posts have shoulders in order to stop the block at a given distance away from the substrate device, allowing the spring loaded probes to press down onto the substrate device at a predetermined position and force. Not only is the device being electrically biased at this

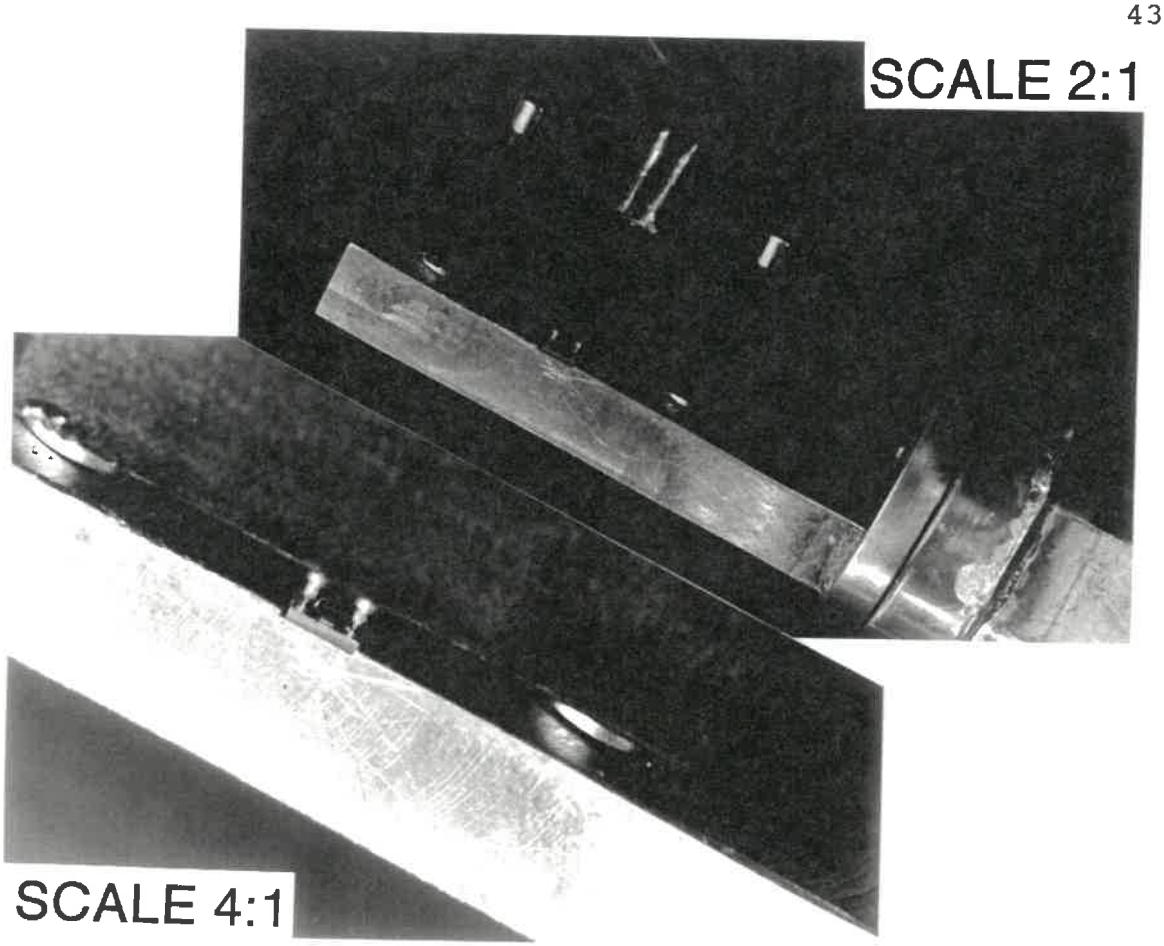

Figure 20. Substrate Device Holder

point, but the force exerted from the probes, ensures some heat sinking to the brass fixture. Electrical leads are soldered to the gold-plated sockets. Again simple patch cords may be used for CW or quasi-CW electrical tests. If high current pulsed tests are required, the termination box is brought as close to these electrical leads as possible. As with other device holders the substrate device holder has provisions for a thermocouple attachment to accurately monitor device temperatures.

3.6.3 Alignment Fixture

Alignment fixtures are the easiest to design. They screw in to the device holder and have their other face nest into the integrating sphere inlet port. Once the inlet port nests into the alignment fixture, the proper positioning of the sphere is found and therefore the reference point for all subsequent cone angle measurements is set. The alignment can be corrected by the use of the 3-axis manipulator and the orientation by rotating the sphere about its support until the face of the inlet port is parallel with the alignment fixture. Figure 21 shows an alignment fixture screwed into a coaxial stud holder.

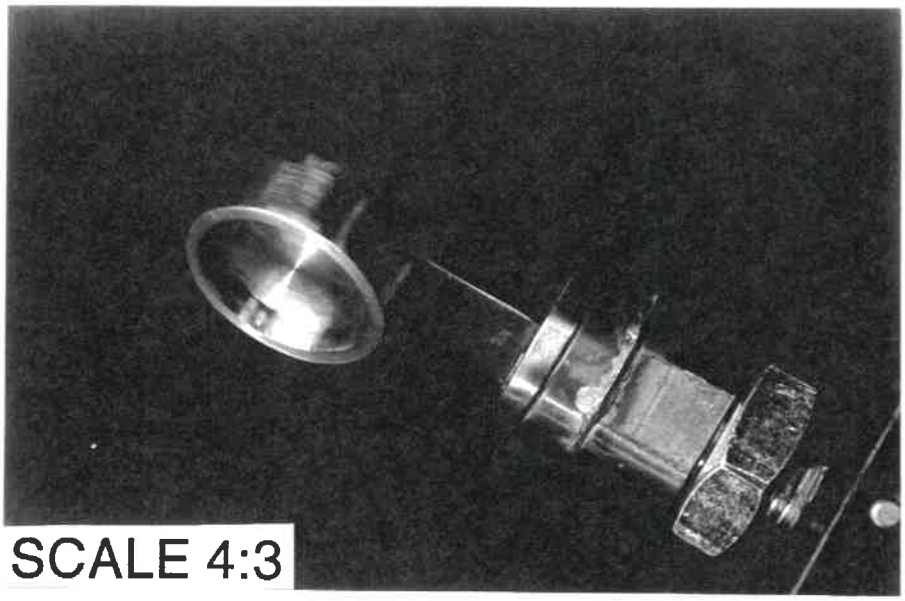

Figure 21. Alignment Fixture

SYNOPSIS

When the integrating sphere test station was first introduced into the production area, it was inevitable to hear both praise and criticism from the supervisors, technicians, operators and production engineers.

The first criticism to be heard was concerned with the inferior manufacturing throughput capabilities of this test station. This station was designed to be accurate and versatile but not necessarily quick. However, with this test station being the norm in our production facility as well as gaining us international recognition, the point is well taken. A lot of the time consumed in testing devices is spent retrieving and engaging the slider which holds the sphere. Right now this is done manually. While disengaging the sphere is readily done, engaging may require some precision of positioning if cone angle measurements are to be taken. For this reason automated sliders with programmable stops have been considered and are deemed compatible with the existing test station. The next generation of this test bench will have automated sliders.

The first praise to be heard targets the ability of this station to test all devices regardless of package style, optical power, nominal wavelength, test temperature or drive current type. By default this station will test all devices

which cannot be tested elsewhere on the manufacturing line. Custom device holders are successful in heat sinking, positioning, orienting and in some cases probing the DUT. Some engineers, however, find that the heat sinking capabilities of the device holders are sub-standard and require work. This fault is being looked into now.

The second criticism comes from the manufacturing engineering department, concerned with the non-ideal behavior of the sphere itself. As the experiments show, the integrating sphere must have its full collection point redefined as well as using an aperture over the 12.7 mm inlet port for accurate cone angle measurements. All of this because the sphere inner skin, at the inlet port, is clipping the entering light. What results are pessimistic measurements of optical power. This problem has been corrected with clever device holders.

Minor complaints about calibration and station operation have been quieted with detailed procedures.

The drawings for all components of this test station are controlled and available from the EG&G drawing office.

REFERENCES

1. Michael Ettenberg, "Laser Diode Systems and Devices", IEEE Circuits and Systems, (September 1987), p.22

2 Laser Diode User Manual, Ref No. HT509D, Sharp Corporation Japan, (September 1988). p.13

3 Optoelectronic Devices Data Book, Ref S30, Hitachi America Ltd., (March 1988), p.60

4 Optoelectronic Devices Data Book, Ref S30, Hitachi America Ltd., (March 1988), p.61

5 Optoelectronic Semiconductors Product Guide, Ref 3636C, Toshiba Corporation Tokyo, (October 1989), p.7

6 Laser Diode User Manual, Ref No. HT509D, Sharp Corporation Japan, (September 1988). p.12

7 Optoelectronic Devices Data Book, Ref S30, Hitachi America Ltd., (March 1988), p.19

8 Optoelectronic Semiconductors Product Guide, Ref 3636C, Toshiba Corporation Tokyo, (October 1989), p.8

9 Optoelectronic Devices Data Book, Ref S30, Hitachi America Ltd., (March 1988), p.62

10 Kevin F. Carr, "Integrating Sphere Flux Calculations", Labsphere Inc. Technical Notes, (September 1988), p 2-3

11 Laser Diode User Manual, Ref No. HT509D, Sharp Corporation Japan, (September 1988). p.26

12 J.P. Holman, Heat Transfer , Mcgraw-Hill Publishing, New York (1986), p. 134

13 F. Kreith, Basic Heat Transfer , Harper & Row Publishing, New York (1980), p. 78

ANNEXES

ANNEX 1

STATION SPECIFICATION

Physical

Size:	64 cm wide X 30 cm deep X 20 cm high
Materials:	aluminium, stainless steel, brass & delrin
Mass:	20 kg

Electrical Drivers

CW:	0 - 500 mA
Quasi-CW:	0 - 6 A, 0 - 200 kHz, 500 ns - 10 ms
Pulsed:	0 - 100 A, 0 - 30 kHz, 80 ns - 1 ms

Optical

- 5.96 cm I.D. integrating sphere with baffle and two 12.7 cm diameter ports @ 90 Degrees to each other
- Silicon photodetector assembly valid from 810 to 940 nm operating linearly up to 7.7 W
- InGaAs photodetector assembly valid from 940 to 1550 nm operating linearly up to 85 W
- 16, 30 and 54 mm extension tubes
- black anodized aperture 6.35 cm in diameter for cone angle measurements varying from 1 to 90 degrees
- fiber bundle exit port for spectral analysis

Thermal

- temperature settings accurate to .1 °C
- 125 to -55 °C capability on most devices
- PID controller ensuring quick settling times
- 4 user programmable temperatures settings
- over temperature sensor

Device Fixtures

- universal socket attachment to temperature controller
- electrical shunt between ground and device holders permitting case positive measurements
- 1 piece brass device holders
- optical alignment fixtures
- provisions for thermocouple attachment on all fixtures
- customized holders for most devices

Manufacturing throughputs (parts/hour)

Full collection + 1 cone inscribed power measurement

Device Type	25°C	-55°C	125°C
Coaxial stud	25	10	12
Transistor Outline	15	8	10
Substrates	15	20	20

ANNEX 2

INTEGRATING SPHERE CALIBRATION PROCEDURE

SCOPE

To outline the steps required to calibrate an integrating sphere for optical power measurements.

EQUIPMENT

- 820nm fibered laser (2-5 mW CW power capability)
- 910nm fibered laser (2-5 mW CW power capability)
- 980nm fibered laser (2-5 mW CW power capability)
- 1060nm fibered laser (2-5 mW CW power capability)
- 1300nm fibered laser (2-5 mW CW power capability)
- 1550nm fibered laser (2-5 mW CW power capability)
- Macom CW laser driver or equivalent
- Anritsu power meter with silicon and germanium heads
- Fiber optic stripper and cleaver
- Fixtures to heat sink and power aforementioned lasers
- Temperature controller
- Various electrical patch cords
- Various tools (allen keys, screwdrivers, etc.)

SAFETY

Warning: Light emitted from optical cable may be

hazardous to eyesight if viewed directly. Use an image converter when viewing light emissions from any light source. Observe ESD precautions

DATA COLLECTION

a) Record the asset number of the integrating sphere, short and long wavelength photodetector assemblies and power meter used on sheet EO-287/92 (Table 1)

b) Place a fibered laser into its electrical and heat sinking fixture. Make the necessary electrical connections between the fixture and the laser current driver.

c) Turn on the power meter and set the wavelength the same as that indicated on the laser. Strip and cleave the end of the fiber optic cable.

d) Hold the cleaved end of the fiber optic cable centered and close to the photosensitive surface of the appropriate photodetector (i.e. silicon for 800 - 920nm and germanium for 980 - 1550nm) and increase the current of the fibered emitter until

Table 1 Integrating Sphere Calibration Data

Sphere # EO - ØØØØ729
Short Wavelength Detector Assembly # EO - ØØØØ1Ø57
Long Wavelength Detector Assembly # EO - ØØØØ68Ø

Optical Power Meter Used: PP-1Ø2Ø425

Atten. Tube	Wavelength											
	TYP:	810	920		980		1060		1300		1550	
	ACT:	818	922		973		1070		1304		1526	
	mV	mW	mV	mW	uA	mW	uA	mW	uA	mW	uA	mW
none												
16 mm	2.69	4.93										
	2.67	4.83										
	2.66	4.74										
30 mm							.913	5.18				
							.925	5.12				
							.905	5.20				
54 mm												

EXAMPLE DO NOT USE

EO 287/92

Date of calibration exercise: JUNE 30, 1992

the power reads between 2 - 5mW.

e) Leaving the drive current unchanged, wait until the optical power stabilizes. Using the spectrometer, determine the center wavelength of the light emitted from the fiber end and record this value on EO-287/92.

f) Verify that the laser is driven well beyond threshold by making sure that the spectral width is less than 10 nm. If not, the drive current will have to be increased and the spectral width remeasured.

g) Adjust the wavelength setting on the power meter to correspond with that found on the spectrometer.

h) At all times, the fibered devices used as light sources must be well heat sunk to avoid possible damage and destruction of these. If the source is equipped with a thermistor and thermoelectric cooler, these may be used in conjunction with a temperature controller to stabilize the case of the source to ambient temperature.

i) Fix the photodetector to the output port of the sphere with no extension tube. Connect the battery to reverse bias the photodetector.

Notes: Silicon photodetector for 810 - 940 nm and reversed biased with 45 Volts. InGaAs photodetector for 940 - 1550 nm and reversed biased with 9 Volts

j) Connect the output of the photodetector to a multimeter. Set the multimeter to read volts for the silicon photodetector and to read amperes for the InGaAs photodetector.

k) Hold the cleaved end of the optical fiber source flush and centered to the inlet port of the integrating sphere. Record the measurement off the multimeter on a copy of sheet EO-287/92.

l) Hold the cleaved end of the fiber optic source cable centered and close to the photosensitive surface of the power meter photodetector. Record the value of the optical power on sheet EO-287/92.

m) Repeat steps k through l another 2 - 4 times depending on the consistency of the results obtained

n) Go back to step i introducing an extension tube between the photodetector and outlet port of the integrating sphere. Repeat steps i through m for each of the three extension tubes.

o) Collection of data is now complete on the given sphere and photodetector assembly for a given wavelength.

p) Repeat steps b through p for all fibered lasers to complete sheet EO-287/92.

q) The collection of data is complete for 6 wavelengths on 4 different extension tubes on a sphere and two mutually exclusive photodetector assemblies. Record the date on EO-287/92

r) Return all fibered lasers to their protective enclosures observing ESD precautions. Disconnect all electrical patch cords and return these along

with fixtures to their place of origin.

CALCULATION OF CALIBRATION FACTORS

a) Record the asset number of the integrating sphere, short and long wavelength photodetectors and power meter used on sheet EO-288/92 (Table 2)

b) For each of the wavelengths at each of the attenuations calculate the calibration factor in the following manner. Divide the sum of the power readings (mW) by the sum of the multimeter readings (uA or mW) to obtain an average ratio in W/A or W/V. These results are to be entered in the CW measurements table of sheet EO 288/92.

c) To complete the pulsed measurement table on EO-288/92 do the following.

d) For wavelengths typically listed at 810 and 920nm multiply the CW measurement result by a factor of 2 and record on the pulsed measurement table of EO-288/92. This is done because the load across the photodetector will be 25 Ohms instead of 50

Table 2 Integrating Sphere Calibration Results

Sphere # EO - 000729
Short Wavelength Detector Assembly # EO - 000001057
Long Wavelength Detector Assembly # EO - 000068Ø

Optical Power Meter Used: PP - 1620425

CW MEASUREMENTS - ASSUMES NO ADDITIONAL LOAD ACROSS DETECTOR OUTPUT

		Wavelength (nm)					
	TYPICAL	810	920	980	1060	1300	1550
	ACTUAL	818	922	973	1070	1304	1526
	CONV. FAC	W/V	W/V	W/A	W/A	W/A	W/A
Atten. Tube	none						
	16 mm	1.81					
	30 mm				5650		
	54 mm						

PULSED MEASUREMENTS - ASSUMES NO ADDITIONAL LOAD ACROSS DETECTOR OUTPUT

EXAMPLE
DO NOT USE

		Wavelength (nm)					
	TYPICAL	810	920	980	1060	1300	1550
	ACTUAL	818	922	973	1070	1304	1526
	CONV. FAC	W/V	W/V	W/V	W/V	W/V	W/V
Atten. Tube	none						
	16 mm	3.62					
	30 mm				113.01		
	54 mm						

Date of calibration exercise: JUNE 30 1992

e) For wavelengths typically listed at 980, 1060, 1300 and 1550nm divide the CW measurement result by a factor of 50 and record on the pulsed measurement table of EO-288/92. This is done because the load across the photodetector will be 50 Ohms instead of none. Notice the units change from W/A to W/V.

f) Record the date at the bottom of EO-288/92

g) Circulate calibration data (EO-287/92) and calibration results (EO-288/92) to appropriate departments (i.e. emitter production, quality and reliability assurance and emitter engineering).

ANNEX 3

INTEGRATING SPHERE TEST STATION OPERATION

SCOPE

To outline the necessary steps in setting up for and performing optical power measurements on a test station using an integrating sphere.

EQUIPMENT

pulsed current source
quasi-CW current source
CW current source
digital thermometer with thermocouple
oscilloscope
multimeter
device holding fixtures
alignment fixtures

SAFETY

Warning: Light emitted from light sources may be hazardous to eyesight if viewed directly. Use an image converter when viewing light emissions from any light source. Observe ESD precautions

MECHANICAL SET-UP

a) Turn on refrigerating unit along with its temperature controller and allow them to initialize for 5 minutes.

b) Place appropriate device holding fixture in the socket of the temperature controller and fasten securely.

c) Using the appropriate alignment fixture, ensure that the device holder is perpendicular to both axes of the face of the inlet port of the sphere. The vernier scale on the slide should read zero when the inlet port of the sphere is nested into the alignment fixture. Adjustments can be made using the manipulators of the 3-axis positioner. The reference point and beam orientation for device light emission have now been established as shown in figure 22.

d) Attach a thermocouple to the back of the device holding fixture. Set the temperature controller to the appropriate temperature keeping in mind

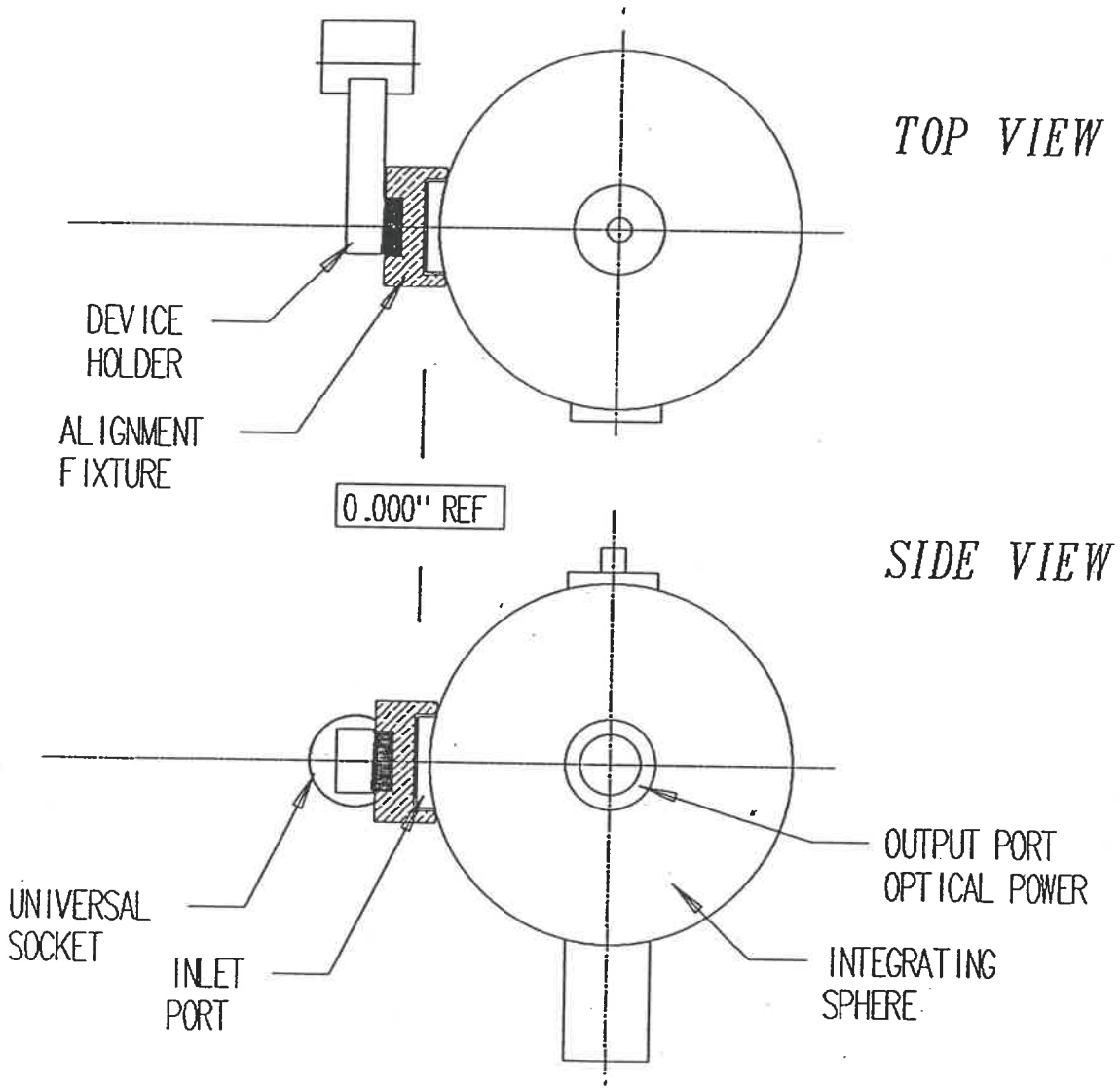

Figure 22. Alignment and Reference Verification

that it is the device holder temperature that is of interest and not that displayed on the temperature controller. The difference is due to the fact that there are convective, conductive and radiative heat losses between the fixture and the environment. Typically the drift is 1/2 degree Celsius per degree Celsius for which the device holder is above or below ambient temperature.

ELECTRICAL SET-UP

N.B. This test station is capable of accommodating high current pulsed , quasi-CW and CW measurements.

Caution: In all cases, respect the polarity of the devices as damage may result to the device and/or current source if a hook-up is improperly done.

a) For quasi-CW and pulsed measurements verify and if necessary adjust the repetition rate and pulse width. Keep in mind that these are measured at the full width half maximum of the test drive current.

b) Electrical connections from the driver to the device are usually done with EZ-clip ended patch cords for quasi-CW and CW measurements.

c) For high current pulsed measurements, the electrical box that terminates the strip line can be fixed, in the back of the device holder, using existing fixtures on the base plate of the test station.

d) Be careful not to exceed the maximum rated current for each current driver and device.

OPTICAL SET-UP

a) Verify that the sphere and photodetector assembly have valid calibration stickers attached to them.

b) Devices emitting light at wavelengths from 800 - 940 nm will be tested using a silicon photodetector assembly, reversed biased at 45 volts.

c) Devices emitting light at wavelengths from 940 -

1600 nm will be tested using an InGaAs photodetector assembly, reversed biased at 9 volts.

d) Consult table 3 to determine which extension tube to use, if any, between the outlet port of the sphere and the photodetector assembly. Proper selection of an extension tube optimizes the signal to noise ratio and guarantees that the photodetector will behave linearly for the power range specified.

e) If the silicon detector assembly is being used, connect its output to a voltmeter for CW

Table 3. Extension Tube Selection

Silicon Photodetector Assembly	
Extension Tube	*Rated Powers*
none	5 – 190 mW
16 mm	190 – 500 mW
30 mm	500 mW – 2.2 W
54 mm	2.2 – 7.7 W

InGaAs Photodetector Assembly	
Extension Tube	*Rated Powers*
none	5 mW – 1.85 W
16 mm	1.85 – 4.80 W
30 mm	4.80 – 20.0 W
54 mm	20.0 – 85.0 W

measurements or to the input channel of an oscilloscope for pulsed or quasi-CW measurements

f) If the InGaAs photodetector assembly is being used, connect its output to an ammeter for CW measurements or to the input channel of an oscilloscope for pulsed or quasi-CW measurements

OPTICAL POWER MEASUREMENTS

a) Place a device in the device holder fixture and make the appropriate electrical connections respecting the polarity of the device.

b) For full collection measurements (i.e. half cone angle of 90 degrees), slide the sphere assembly over such that the inlet port of the sphere contacts the back of the device holder.

c) For cone inscribed optical power measurements, calculate the distance, X (in mm), the slider must be pushed back with the following formula.

X = 3.175 / Tan (cone 1/2 angle required)

Place the 6.35mm aperture over the inlet port of the sphere

d) Slowly increase the drive current to the desired value.

e) Read the output of the detector and refer to the appropriate CALIBRATION RESULTS sheet (EO-288/92) to obtain the proper transfer characteristic (i.e. W/A or W/V). Multiply the reading of the photodetector output by this transfer characteristic to obtain a result in Watts.

f) Record this power measurement on the test record sheet called out on the work order.

g) Lower drive current to zero and remove the device. Warning: Removing device with current still on may cause damage to the current driver or device.

h) Repeat for as many devices as require testing.

ANNEX 4

INTEGRATING SPHERE CHARACTERIZATION

The following experiments were conducted to verify that the integrating sphere output is accurate.

FULL COLLECTION AND CONE INSCRIBED POWERS

The following issue was brought forth: the sphere internal reflective coating (essentially a packed white powder), at the proximity of the inlet port, might be acting as a limiting aperture, due to its thickness. Concerns were voiced that full collection and cone inscribed power measurements could be biased (i.e. lower powers read).

The first part of the experiment seeks to determine at which point between the face of the inlet port and the sphere inner surface a laser diode chip would produce maximum photodetector output. Using the sphere inner surface as the reference, we can see from table 4 that the optimal position is 5 mm from the sphere inner skin towards the inlet port as shown in figure 23.

The second part of the experiment seeks to determine the differences, in photodetector output, for cone inscribed powers between the light seen through the sphere 12.7 mm inlet port and through a 6.35 mm aperture laid flush and

Table 4 Output vs Outward Distance from Sphere Inner Skin

Distance (in mm)	Millivolts read off detector output			Percent Collection
	1st run	2nd run	Avg	
0.0	19.7	19.5	19.6	97.0
2.5	19.9	19.8	19.8	98.2
3.8	20.0	20.0	20.0	98.9
5.0	20.2	20.2	20.2	100.0
6.3	20.0	20.0	20.0	99.0
7.5	18.9	19.1	19.0	93.9
10.5	17.3	17.3	17.3	85.7

concentric to the inlet port of the sphere. Table 5 shows greater photodetector output for the 6.35 mm aperture for all cone angles tested.

Conclusions / Recommendations

We are presently referring to the front face, of the sphere inlet port, as the reference point (0.000) and assuming incorrectly that this is the full collection point. Whenever possible, full collection measurements should be made with the emitting chip halfway between the sphere inner skin and inlet port face. Assuming the inlet port face to be the full collection point leads to an error of 14.3 percent. As it was suspected the inner surface of the sphere is "clipping" some of the entering light. It is

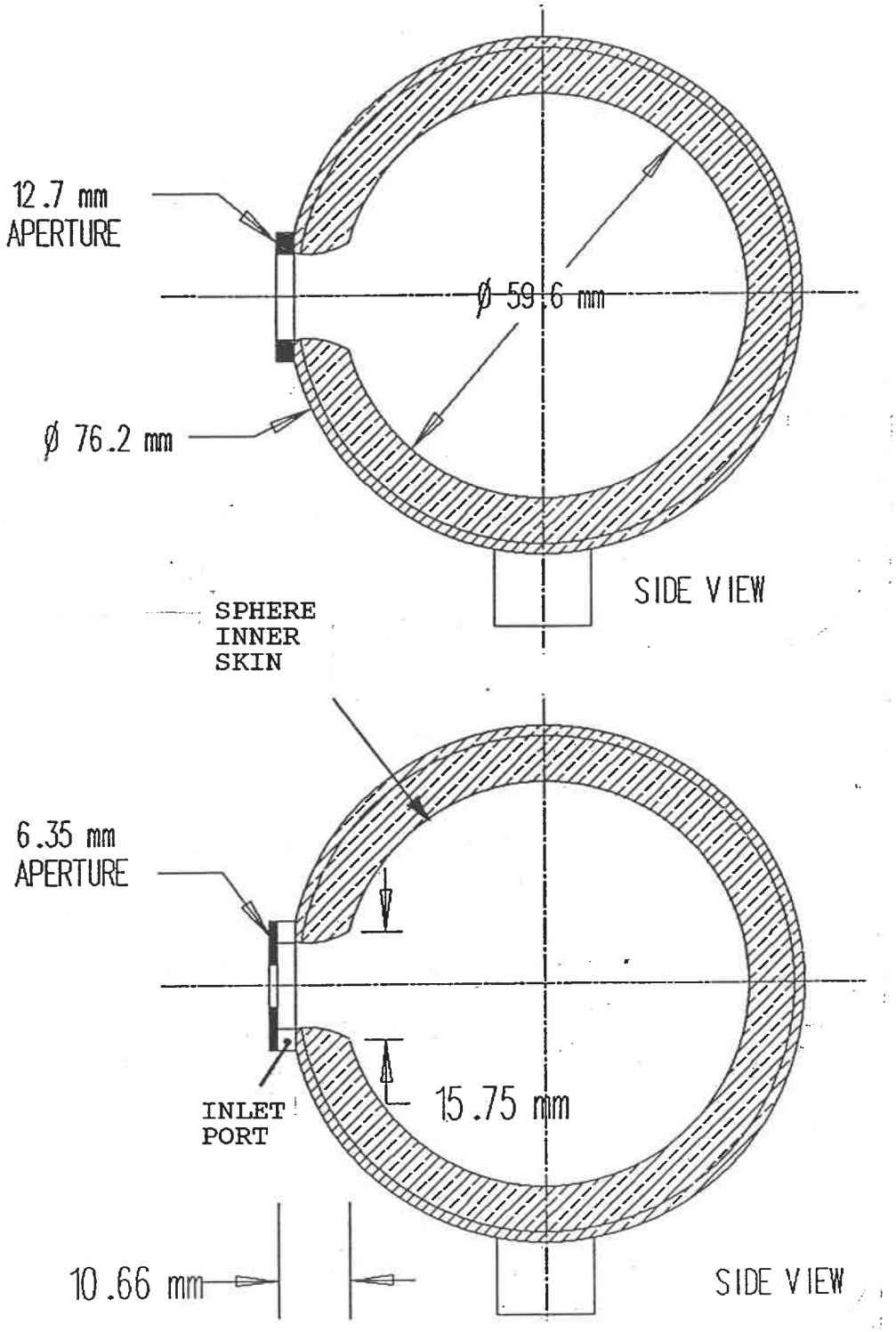

Figure 23 Integrating Sphere with 12.7 and 6.35 mm Apertures

Table 5 Comparison of Optical Apertures

	Millivolts read off detector output		
Cone angle in degrees	12.7 mm aperture	6.35 mm aperture	percent difference
10	5.3	5.8	9.9
20	10.1	11.3	12.0
30	12.6	13.9	10.3
40	14.2	15.2	7.4
50	15.0	15.8	5.3
60	15.7	16.2	3.2
70	16.2	16.5	1.7
80	16.7	16.8	0.4

recommended to use a 6.35 mm aperture when making cone inscribed power measurements. As seen from table 5, the error in relying on the 12.7 mm aperture is significant.

PHOTODETECTOR LINEARITY

The basis for accurate light measurement is photodetector linearity. It is important to determine the range of operation over which a calibration factor can be considered to be valid. The reader is reminded that the integrating spheres are calibrated at low power (typically 5 mW) using CW fibered light sources and typically operate at several Watts pulsed power. By shining a light source on a calibrated large area photodiode and then shining the same

light source on the integrating sphere photodetector we can obtain a ratio. These ratios will be the same regardless of power if the photodetector being tested is operating linearly. In the case at hand, both the long and short wavelength detectors are verified for linearity. The limit of linearity is not found in either case since the constant current light sources used are limited in power. As can be seen from figure 24, we can, however, say that the long and short wavelength photodetectors are at least linear up to 6 and 11 mW respectively. The reader is reminded that these are not the limit input powers into the sphere since only a small fraction of the entering light is incident onto the affixed photodetector. Typically only .1 percent of the light emitted into the sphere inlet port will be incident onto the affixed photodetector assembly. In this case, the sphere could be said to operate linearly from 0 to 6 Watts at long wavelengths and from 0 to 11 Watts at short wavelengths. The actual throughputs of the sphere, measured with different extension tubes will be used to accurately evaluate the maximum incident optical power any one configuration should be allowed to accept. The rated limits for input optical power, into the sphere, are tabulated in Annex 3 (Integrating Sphere Test Station Operation)

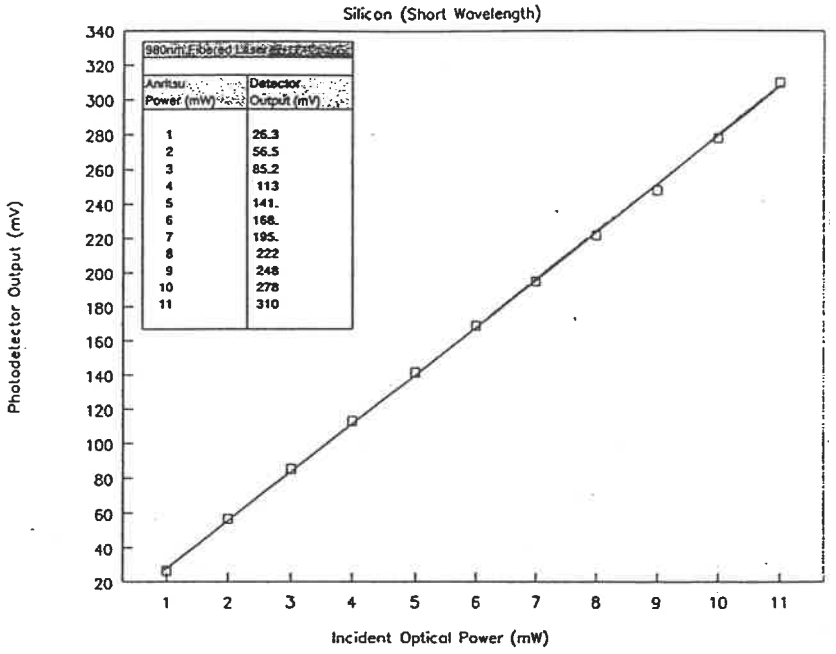

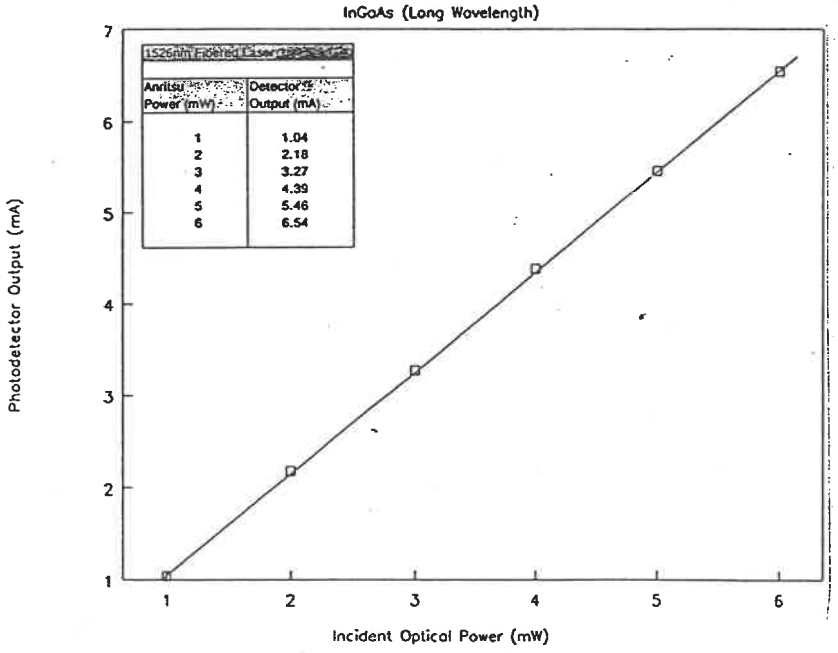

Figure 24 Silicon and InGaAs Photodetector Linearity

INTEGRATING SPHERE THROUGHPUTS

Ever since the equations provided by the integrating sphere manufacturer yielded theoretical throughputs well below (5 times less) those measured at EG&G Optoelectronics, many engineers and technicians were left puzzled and annoyed.

Labsphere, the integrating sphere manufacturer, could shed no light on this mystery.

Another look at Labsphere's application notes reveals that the theory assumes non-reflective ports. The photodetector holder on the exit port is non-reflective but the throat of both ports, leading from the sphere inner to outer skin is reflective. Could such a comparatively small reflective surface be responsible for such a large error ? The following experiment proves it is.

Much like when the spheres are calibrated, a fibered light source emitting nominally 5mW of optical power into the inlet port of the sphere produces an output across the photodetector affixed onto the outlet port. Results can be found in table 6. The same experiment is repeated with the

Table 6 - Throughput vs Port Reflectivity

	Reflective Ports		Non-Reflective Ports	
RUN	P_i(mW)	P_o(uW)	P_i(mW)	P_o(uW)
1	4.92	12.24	5.00	3.89
2	4.89	12.35	4.63	3.74
3	4.69	12.43	4.79	3.68
4	4.83	12.13	4.75	3.97
5	4.85	11.92	4.73	3.95
AVG	4.84	12.21	4.78	3.85

presence of blackened shrouds over the reflective surfaces of the ports as well as over the face of the inlet port as shown in figure 25. These results are also tabulated in table 6. P_i and P_o designate input optical power and optical power collected by the photodetector respectively.

Dividing P_o by P_i yields actual throughput measurements.

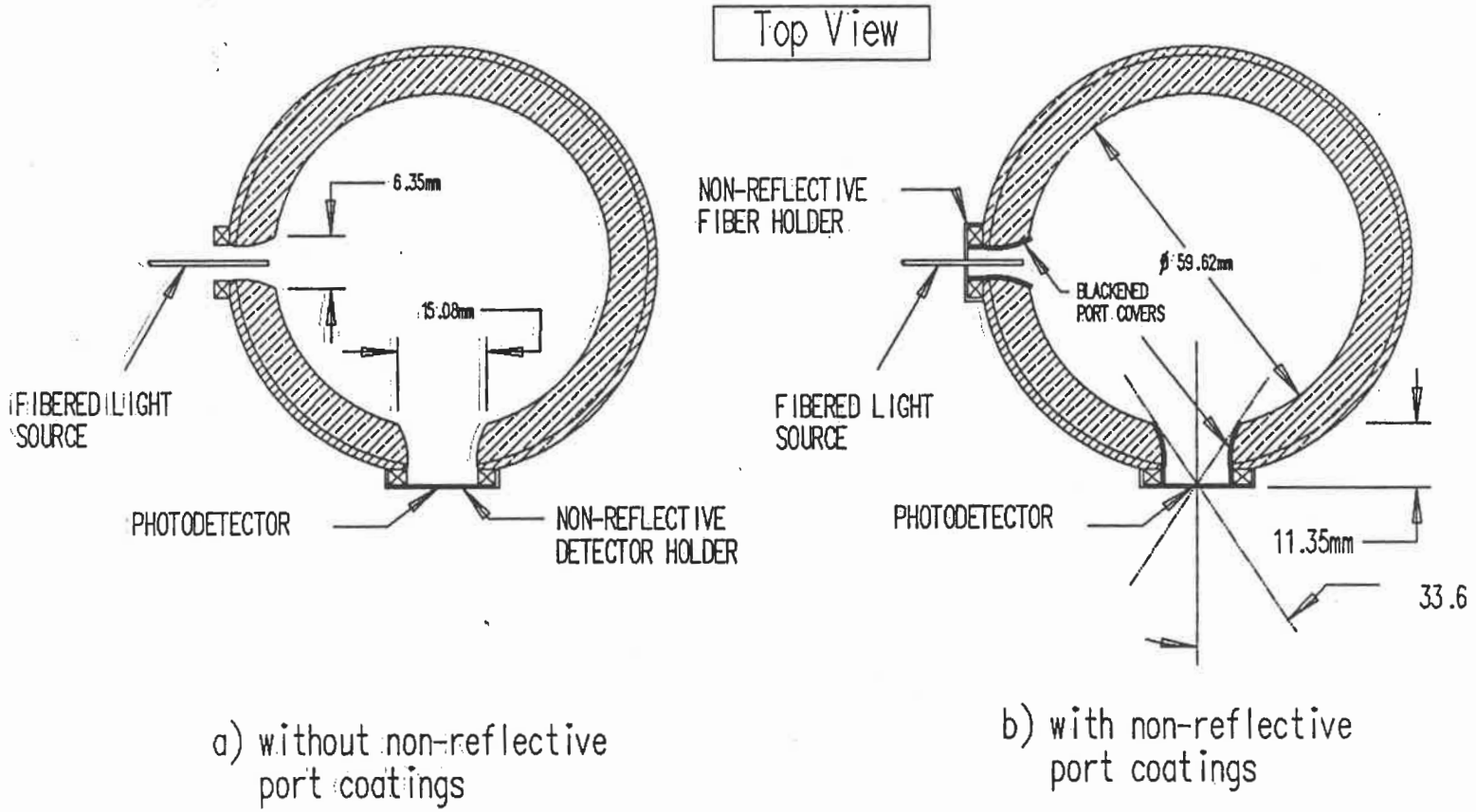

Figure 25 Cross Section of the EG&G Integrating Sphere

The sphere with reflective ports has an average throughput of 2.52E-3 whereas the same sphere with its ports made non-reflective has an average throughput of .805E-3.

Surprisingly enough, the output has changed by a factor of three. As mentioned earlier on, theoretical calculations yielded throughputs five times less than those measured. The remainder of the error is attributed to the change in output port size. (i.e. the addition of blackened shrouds redefines the diameter of the output port taken at the sphere inner skin.)

The theoretical throughput calculated from equations 1 to 8, is .833E-3. This represents an error of 3.4% with the actual throughput (.805E-3). This error is acceptable since most of the critical dimensions, such as the diameter of the sphere's inner skin and exit port areas are difficult to measure accurately. It's also much more comforting to observe higher theoretical than actual throughputs.

Conclusion/Recommendation: Future purchase orders for integrating spheres should specify the ports (inlet and outlet) to be entirely non-reflective.

ANNEX 5

THERMAL PERFORMANCE

When the mechanical interface between the device and the heat exchanger was first designed, the concept held as most important was its thermal performance. The criteria for accepting the system, based on its thermal performance, is as follows:

1. - The ability to operate at device temperatures ranging from -55°C to 125°C

2. - The ability to monitor the device temperature to within a 3°C accuracy

3. - Ensure that the misalignments caused by thermal expansions are negligible

The purpose of this analysis is then to validate its preliminary design.

TEMPERATURE CONTROLLED HEAT EXCHANGER

The analysis begins by characterizing the heat exchanger. The following information is given by the manufacturer.

Table 7 - Heat Extraction Capability

0	Watts at -80 °C
5	Watts at -55 °C
50	Watts at 25 °C
100	Watts at 125 °C

Table 8 - Heat Generation Capability

5	Watts at -55 °C
50	Watts at 25 °C
100	Watts at 125 °C

A regression analysis yields the following relationships:

Heat extraction = .503 W/°C X Temp(°C) + 36.86 W (9)

(regression coefficient of .997)

Heat generation = .526 W/°C X Temp(°C) + 34.98 W (10)

(regression coefficient of .999)

The driving functions having been converted from a

series of discreet points to simple equations, it is possible to proceed to the heat transfer analysis.

LUMPED HEAT CAPACITY ANALYSIS

Transient heat conduction problems can be solved by a lumped heat capacity analysis when the following is true.[12]

$$\text{Biot Number} = hv / ka < .1 \qquad (11)$$

where h is the convective heat transfer in W/ $m^2 \cdot C$

v is the volume of material in m^3

k is the material thermal conductivity in W/ $m \cdot C$

a is the total convective surface area in m^2

Figure 26 shows the thermal path between the device and the heat exchanger probe. The geometry of the assembly having already been determined by the environment it rests in as well as the purpose it serves, the choice of material is the only parameter that has not been yet fixed. Brass, reknown for its ease of machining, good thermal conductivity and commercial availability will be used as the test material for this analysis.

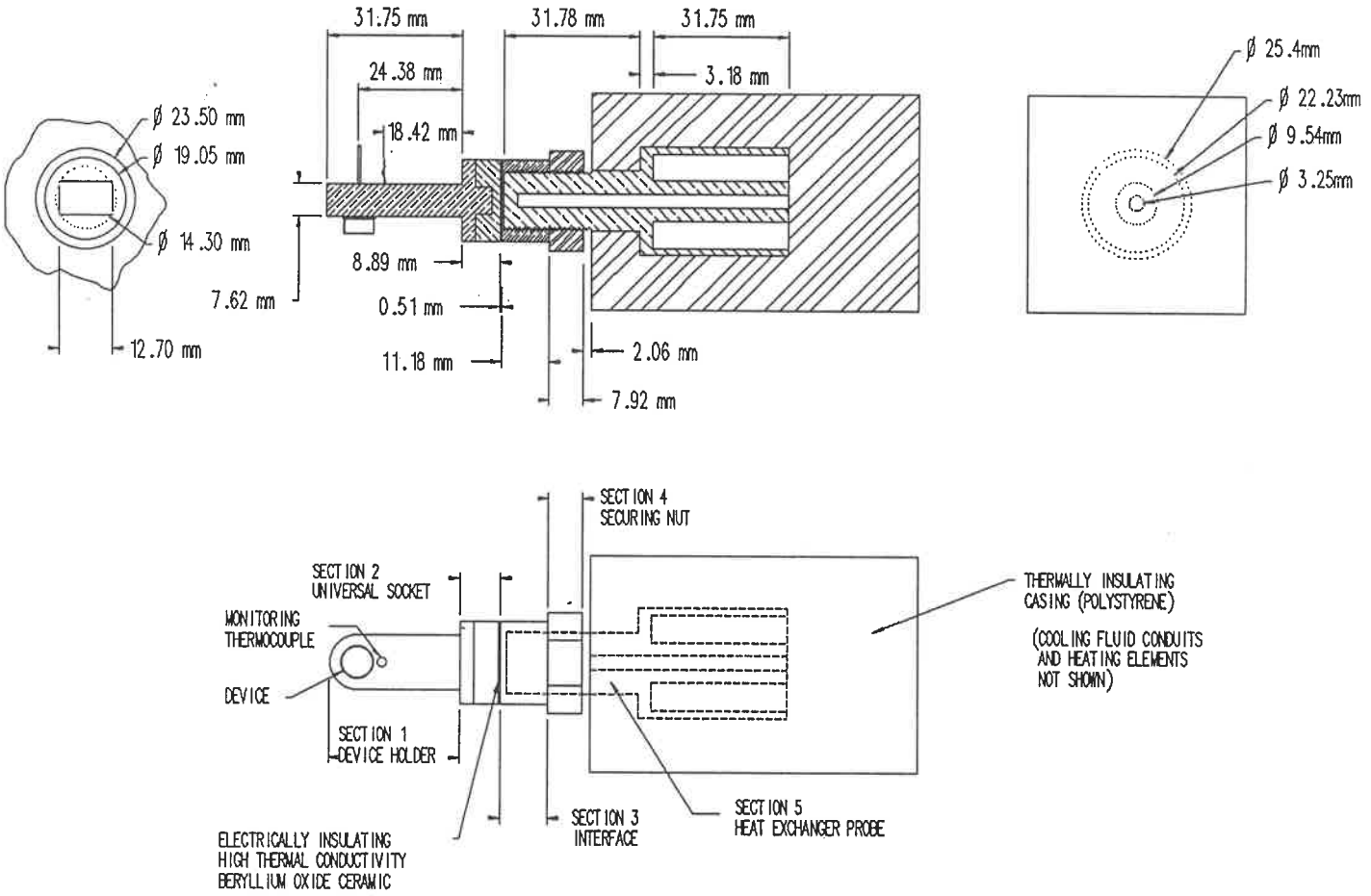

FIGURE 26: TEMPERATURE CONTROLLER PROBE WITH FIXTURES

For the purpose of this analysis, it can be safely assumed that the entire assembly is a one piece fixture since the thin electrically insulating ceramic is of higher thermal conductivity than brass and that the thermal contact resistance between the mating parts is negligible as it will be later shown.

Proceeding with the analysis, the volumes and convective surface areas of each section, as depicted in Figure 26, are tabulated below.

Table 9 - Volumes and Convective Areas of Fixtures

Section	Volume (mm^3)	Areas (mm^2)
1	2941	1311
2	2103	630
3	1393	670
4	2186	1012
5	12171	143
Total	20794	3766

Typically, convective heat transfer coefficients vary from 5 to 25 W/ m^2 °C for natural convection as is the case. The lowest thermal conductivity of any material (stainless steel) used in this assembly is 15 W / m°C.

Assuming worst case (i.e. h = 25 W/ m^2 °C and k = 15 W/ m°C), the result for the Biot number is calculated to be:

$$\frac{25\ W/\ m^2\ °C\ *\ 20.794\ X\ 10^{-6} m^3}{15\ W/\ m°C\ *\ 3.766\ X\ 10^{-3} m^2} = .009 \qquad (12)$$

The result for the Biot number is well below the maximum allowed of .1 and the lumped heat capacity analysis is proved to be applicable.

THERMAL CONTACT RESISTANCE

Typical thermal contact resistance for ground machined surfaces, as in this assembly, is .07 X 10^{-4} m^2 °C / W.

The smallest contacting area is at the mating point between section 1 & 2. Its surface is calculated to be:

$$\frac{\pi(19.05\ X\ 10^{-3} m)^2}{4} + \pi * .0038 * .00635m \qquad (13)$$

$$= .00036m^2$$

The maximum heat flow the heat exchanger can produce is 100 Watts as shown in tables 7 & 8.

The temperature drop across the interface is then:

$$100\ W\ *\ \frac{1}{.00036 m^2}\ *\ .07\ X\ 10^{-4}\ \frac{m^2\ °C}{W}\ =\ 1.9°C \qquad (14)$$

The use of thermal grease between mating surfaces is known to reduce the contact resistance by at least 1/2 of its original value. For the assembly in question, this would result in less than a 1 degree (.95 °C) loss between mating surfaces. Since the analysis deals with differences of 100°C, a loss of such small magnitude is certainly considered to be negligible.

TRANSIENT HEAT TRANSFER

Having proven the applicability of the lumped heat capacity we proceed with the governing equation.

$$q_{he} - q_{conv} = \Sigma Cpv\ dT/dt \qquad (15)$$

where q_{he} is the heat generated or extracted in Watts

q_{conv} is the convected heat in Watts

C is the specific heat in J/ kg°C

p is the density of the material in kg/m^3

v is the volume of the material in m^3

T is the fixture temperature in °C

t is the time in seconds

Since the extraction and generation of heat are both defined by different linear equations, we let $q_{he} = mT + b$ and adopt the following sign convention:

Heat extraction is equal to -.503 W/°C X Temp(°C) - 36.86 W

Heat generation is equal to +.526 W/°C X Temp(°C) + 34.98 W

The governing equation, in Watts, then becomes:

$$(mT + b) - ha(T-T_\infty) = \Sigma Cpv\ dT/dt \qquad (16)$$

Solving for dT/dt, in °C/s yields:

$$dT/dt = \frac{(m*T + b) - ha*(T-T_\infty)}{\Sigma Cpv} \qquad (17)$$

$$dT/dt = \frac{(m-ha)*T + b + haT_\infty}{\Sigma Cpv} \qquad (18)$$

Equation 18 is integrated to solve for time as a function of temperature. Let i = m-ha and j = b+ haT_∞ to reduce clutter.

$$\int_{T_1}^{T_2} \frac{\Sigma Cpv \, dT}{iT + j} = \int dt \qquad (19)$$

The integration yields the following:

$$\delta t = \frac{\Sigma Cpv}{i} \ln\left(\frac{iT_2 + j}{iT_1 + j}\right) \qquad (20)$$

To determine the cycle time from 25°C to -55°C the following parameters are used.

mT + b is equal to -.503 W/°C X Temp(°C) - 36.86 W

T_∞ is 25 °C (ambient)

h = 25 W/ m² °C

a = 3766 mm²

T_1 = 25 °C

Accounting for all the different materials present:

Brass: C=385 J/kg°C, p=8522 kg/m^3, v=6437 mm^3

Copper: C=383 J/kg°C, p=8954 kg/m^3, v=12171 mm^3

Stainless Steel: C=452 J/kg°C, p=7897 kg/m^3, v=2186 mm^3

ΣCpv = 70.66 J / °C

$i = -.503\ W/°C - 25\ W/\ °C\ m^2\ *\ 3766\ X\ 10^{-9} m^2 = -.6\ W/°C$

$j = -36.86\ W + 25\ W/\ °C\ m^2\ *\ 3766\ X\ 10^{-9} m^2\ *\ 25°C = -34.50\ W$

Resorting to equation 20 we calculate a theoretical cycle time of:

$$\delta t = \frac{70.66}{-.597} * \ln\left(\frac{-.597 * -55 - 34.50}{-.597 * 25 - 34.50}\right) = 401\ s$$

Actual cycle times for this process have been measured to be 380 seconds (i.e. less than 7 minutes)

A similar calculation is made to determine cycle time from 25°C to 125°C using the heat generation equation (i.e. +.526 W/°C X Temp(°C) +34.98) whereas all other parameters remain the same.

Resorting to equation 20 again yields a theoretical cycle time of:

$\delta t\ (T_2 = 125°C,\ T_1 = 25°C) = 105$ seconds

Actual cycle times for this process have been measured to be 95 seconds (i.e. less than 2 minutes)

DEVICE TEMPERATURE MONITORING ACCURACY

Section 1, as shown in Figure 26, is of prime interest since it holds both the device and thermocouple monitoring its temperature.

Using available equations quantifying the heat loss and temperature distribution of fins of uniform cross section, we proceed to find these for the fin (i.e. section 1).

Since the end of the fin is rounded we need to replace it by a length of similar cross section. The fin convective surface area has been calculated to be 1311mm²

The equivalent length for a fin of the same cross section, maintaining the same convective area would be:

$$\frac{1311\text{mm}^2 - WXH}{2*(W*H)} = 29.9\text{mm} \qquad (21)$$

where W is the width of the fin (7.62mm)

H is the height of the fin (12.7mm)

The temperature distribution along a fin of uniform cross section, as shown in figure 27, is given by [13]:

$$\theta(\delta) = \frac{T(\delta) - T_\infty}{T_b - T_\infty} \tag{22}$$

$$\theta(\delta) = \frac{\cosh[\sqrt{}^2 Bi*(1-\delta)] + \sqrt{}^2 Bi*A/PL*\sinh[\sqrt{}^2 Bi*(1-\delta)]}{\cosh \sqrt{}^2 Bi + \sqrt{}^2 Bi*A/PL*\sinh \sqrt{}^2 Bi} \tag{23}$$

where $\delta = x/l$ (dimensionless)

$Bi = h*P*l^2 / (k*A)$ (dimensionless)

$T_\infty = 25°C$

T_b = fin base temperature in °C

P = perimeter of fin cross-section in m

l = length of fin .0299 m

h = convective heat transfer 25 W / m^2 °C

k = material thermal conductivity in W / m°C

A = fin cross sectional area in m^2

a = convective surface area in m^2

x = distance from the base of the fin in m

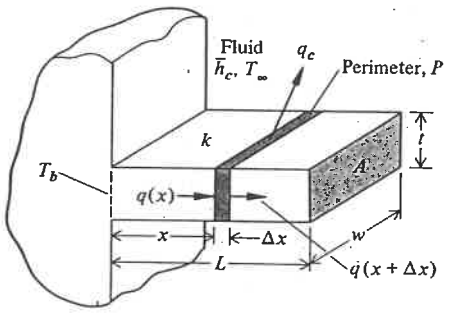

Figure 27 Fin with constant cross-section [13]

The device is located 24.1mm from the base of the fin whereas the monitoring thermocouple is 18.4mm from the base. Assuming the extreme case (125°C device temperature with an ambient of 25°C) the fin base temperature is calculated at a device temperature of 125°C

δ = 24.1mm / 29.9 mm = .806

$1-\delta$ = .194

Bi = 25 W/m² °C * 40.64mm * 29.9mm²/(110 W / m°C * 96.77mm²)

= .0853

$\sqrt{2}$ Bi = .292

A/Pl = .0796 (dimensionless)

Using equation 23 and the values above we find:

$$\theta(\delta) = \frac{\cosh[.292*.194] + .292*.0796*\sinh[.292*.194]}{\cosh .292 + .292*.0796*\sinh.292}$$

$$= .955 = \frac{125°C - 25°C}{T_b - 25°C}$$

$$T_b = 129.7°C$$

Having the fin base temperature (129.7°C), the temperature monitored by the thermocouple 18.4mm (δ = .615) from the base can be calculated from the same equations to be 125.6°C. This represents less than a 1°C error in monitoring. At the other extreme (-55°C device temperature

with an ambient of 25°C), the fin base temperature would be -58.7°C whereas the temperature monitored by the thermocouple would be -55.4°C

The base temperature having been determined, the heat losses can be calculated, in Watts, with the following equation to quantify how accurate the lumped heat capacity analysis has been.

$$q_f = \frac{\sqrt{2}\,Bi*k*A*(T_b-T_\infty)}{l} * \frac{\sinh \sqrt{2}\,Bi + \sqrt{2}\,Bi*A/PL*\cosh \sqrt{2}\,Bi}{\cosh \sqrt{2}\,Bi + \sqrt{2}\,Bi*A/PL*\sinh \sqrt{2}\,Bi} \quad (24)$$

Solving equation 24 for fin base temperatures of 129.7°C and -58.7 yields heat losses of 3.33 and -2.66 Watts respectively.

With the lumped heat capacity analysis, the fin heat losses would be calculated in the following way.

$$q_f = ha\ (T_{device}-T_\infty) \quad \text{in Watts} \quad (25)$$

Equation 25 would yield losses of 3.27 W and -2.62 W for device temperatures of 125°C and -55°C respectively. Both heat losses, calculated with the lumped heat capacity analysis show less than a 2 percent error against the theoretical fin analysis.

THERMAL EXPANSION

Thermal expansion will cause misalignments which may be unacceptable. It remains to determine if these misalignments, characterized by the equation below are significant.

$$\delta l = l * TEC * \delta °C \qquad (18)$$

where δl = change in length in m

l = length of assembly in m

TEC = thermal expansion coefficient in m/m °C

$\delta °C$ = change in temperature in °C

The assembly is approximately .05m long and has components whose worst thermal expansion coefficients will not surpass 22E-6 m/m °C. The assembly sees a maximum temperature differential of 105°C (i.e. 129.7°C - 25°C) The change in length, calculated from equation 20, is equal to .11mm. This change is negligible

Conclusion / Recommendation

It has been seen from the previous analysis that a

device holder and universal socket constructed of brass, along with a securing steel nut will allow the previously established objectives to be met. A prototype was built and tested and the verdict was the same: brass is a suitable material to meet the thermal performance objectives of this test station.

ANNEX 6

STATION COSTING

The following are cost estimates (in Canadian dollars) from previous purchase orders and are based on low quantities (5 or less of each)

A. Basic Features

- 76.2 mm diameter sphere with two 12.7 mm ports	$2 000
- robust 3 axis positioner	$1 500
- axial slide with vernier scale	$ 500
- black anodized aluminum base plate 30 cm X 60 cm	$ 250
- rigid temperature controller support	$ 300
- temperature controller dummy + universal socket	$ 200
- sphere and electrical driver support + misc jigging	$ 400
Sub-Total	$5 150

B. Integrating Sphere Accessories

- extension tubes 16, 30, and 54 mm	$ 600
- InGaAs photodetector assembly with calibration	$ 700
- silicon photodetector assembly with calibration	$ 500
Sub-Total	$1 800

C. Electrical Drivers

- pulsed current source	$3 000
- CW current source	$2 000
- quasi-CW current source	$1 000
Sub-Total	$6 000

D. Temperature Controller

- conduction type valid from -55°C to 125°C	$9 000
- conduction type valid from -46°C to 125°C	$8 000

E. Device Fixtures

- coaxial stud holders	$ 100
- transistor outline holders	$ 200
- substrate holders	$ 300
- alignment jig	$ 100

F. Options

- optical fiber holder	$ 500
- axial slide with electronic position readout	$2 000

ANNEX 7

MARKETABILITY

Research has shown that only one other corporation sells a system using integrating spheres to characterize semiconductor laser diodes. This corporation who shall remain nameless, for legal reasons, once customized a test station to evaluate 9mm CD (Compact Disc) packaged lasers. The application was very specific and did not catch on commercially. We can nevertheless compare their system to ours.

	Theirs	EG&G's
Max. drive current CW	200 mA	2 A
Max. drive current pulsed	200 mA	100 A
Max. drive current quasi-CW	Not Capable	6 A
Minimum pulse width	500 ns	80 ns
Maximum pulse width	-	10 ms
Accuracy of Measurement	5 %	5 %
Maximum device temperature	100°C	125°C
Minimum device temperature	-20°C	-55°C
Far Field Measurements	Capable of	Not Capable

Cone Angle Measurements	Capable of	Capable of
Spectral Analysis	Integrated	Capable of
Automated Testing	Capable of	Incapable of
Basic Cost	$160 000	$27 000

In essence their system failed for 3 reasons. Most of the semiconductor lasers sold today operate at currents (i.e. 10 A pulsed min) far in excess of what their system is capable of. The second reason is that many semiconductor lasers are sold for military applications where tests at -55°C as well as 85°C are required. The cooling system they use (2 cascaded Peltier heat pumps) provides for a minimum of -20°C. The inability of their system to change over from one package style to another is the third reason their test bench failed. The EG&G station can change over from one package style to another in less than 60 seconds.

Far field measurements are typically done on a sample basis (i.e. < 1%). This option on their system is useful but much more for an R&D environment than manufacturing

work.

The practical aspect of their system is automated testing. Data acquisition and software controlled tests are very attractive, but at what cost? It is our opinion that their system is a complete station capable of all tests, but not to the limits required (i.e. limited drive currents, device temperatures and package versatility). Their system lacked the "muscle" to compete in the marketplace and was simply too expensive.

EG&G is already quoting European and Asian firms for our system. This is quite impressive since our system was destined for internal use only two years ago. It seems we have filled a need in the optoelectronics community (i.e. repeatable accurate optical power measurements on diodes at any drive current, any temperature in any package.)